Steps toward determination of the size and structure of the broad-line region in active galactic nuclei. II - an intensive study of NGC 5548 at optical wavelengths

THE ASTROPHYSICAL JOURNAL, 368:119–137, 1991 February 10

STEPS TOWARD DETERMINATION OF THE SIZE AND STRUCTURE OF THE BROAD-LINE REGION IN ACTIVE GALACTIC NUCLEI. II. AN INTENSIVE STUDY OF NGC 5548 AT OPTICAL WAVELENGTHS

B. M. PETERSON,[1,2] T. J. BALONEK,[3] E. S. BARKER,[4] J. BECHTOLD,[5] R. BERTRAM,[1] N. G. BOCHKAREV,[6] M. J. BOLTE,[7] D. BOND,[7] T. A. BOROSON,[8,9] M. T. CARINI,[10] T. E. CARONE,[11] J. A. CHRISTENSEN,[3] S. D. CLEMENTS,[12] A. L. COCHRAN,[4] R. D. COHEN,[13] D. CRAMPTON,[7] M. DIETRICH,[14] M. ELVIS,[15] A. FERGUSON,[7] A. V. FILIPPENKO,[16] K. J. FRICKE,[14] C. M. GASKELL,[17] J. P. HALPERN,[18,19] J. P. HUCHRA,[15] J. B. HUTCHINGS,[7] W. KOLLATSCHNY,[14] A. P. KORATKAR,[17] K. T. KORISTA,[1] J. H. KROLIK,[20] N. J. LAME,[1] A. LAOR,[21] R. J. LEACOCK,[12] G. M. MACALPINE,[17] M. A. MALKAN,[22] D. MAOZ,[21] H. R. MILLER,[10] S. L. MORRIS,[8] H. NETZER,[21] C. L. M. OLIVEIRA,[23] J. PENFOLD,[24] M. V. PENSTON,[25] E. PÉREZ,[26] R. W. POGGE,[1,4] M. W. RICHMOND,[16] W. ROMANISHIN,[27] E. I. ROSENBLATT,[22] L. SADDLEMYER,[7] A. SADUN,[28] S. R. SAWYER,[4] J. C. SHIELDS,[16] A. I. SHAPOVALOVA,[29] A. G. SMITH,[12] H. A. SMITH,[30] P. S. SMITH,[5] W.-H. SUN,[31,32] U. THIELE,[33] T. J. TURNER,[34] S. VEILLEUX,[2] R. M. WAGNER,[1] R. J. WEYMANN,[8] B. J. WILKES,[15] B. J. WILLS,[4] D. WILLS,[4] AND P. F. YOUNGER[7]

Received 1990 June 29; accepted 1990 August 3

ABSTRACT

We report on a large, international program of ground-based optical spectroscopy and photometry of the variable Seyfert 1 galaxy NGC 5548 undertaken in support of an *IUE* monitoring campaign described by Clavel and coworkers. In this contribution, we present the data base and describe the methods used to correct for systematic differences between spectra from different sources. Optical continuum and Hβ emission-line light curves are derived from the spectra. The behavior of the optical continuum is qualitatively the same as the behavior of the ultraviolet continuum. Cross-correlation of the ultraviolet and optical continuum measurements does not reveal any significant lag between them. The Hβ emission-line variations show the same basic pattern as seen in the continuum and ultraviolet emission lines, with Hβ lagging behind the continuum by $\sim$20 days. This is significantly larger than the $\sim$10 day lag deduced for Lyα.

Subject headings: galaxies: individual (NGC 5548) — galaxies: Seyfert — spectrophotometry

[1] Department of Astronomy, The Ohio State University.
[2] University of California Observatories/Lick Observatory, University of California, Santa Cruz.
[3] Department of Physics and Astronomy, Colgate University.
[4] McDonald Observatory and Department of Astronomy, University of Texas at Austin.
[5] Steward Observatory, University of Arizona.
[6] Sternberg State Astronomical Institute, University of Moscow.
[7] Dominion Astrophysical Observatory, National Research Council of Canada.
[8] Observatories of the Carnegie Institution of Washington.
[9] Kitt Peak National Observatory, National Optical Astronomy Observatories.
[10] Department of Physics and Astronomy, Georgia State University.
[11] Lunar and Planetary Laboratory–West, University of Arizona.
[12] Rosemary Hill Observatory, University of Florida.
[13] Center for Astrophysics and Space Sciences, University of California, San Diego.
[14] Universitäts-Sternwarte Göttingen.
[15] Center for Astrophysics, Smithsonian Astrophysical Observatory.
[16] Department of Astronomy, University of California, Berkeley.
[17] Department of Astronomy, University of Michigan.
[18] Department of Astronomy, Columbia University.
[19] Visiting Astronomer, Kitt Peak National Observatory, National Optical Astronomy Observatories, which is operated by AURA, Inc., under a cooperative agreement with the National Science Foundation.
[20] Department of Physics and Astronomy, Johns Hopkins University.
[21] School of Physics and Astronomy and the Wise Observatory, Tel-Aviv University.
[22] Department of Astronomy, University of California, Los Angeles.
[23] Department of Astronomy, University of British Columbia.
[24] Department of Mathematics, Physics, and Engineering, Mount Royal College.
[25] Royal Greenwich Observatory.
[26] Instituto de Astrofisica de Canarias.
[27] Department of Physics and Astronomy, University of Oklahoma.
[28] Department of Physics and Astronomy, Agnes Scott College.
[29] Special Astrophysical Observatory, USSR Academy of Sciences.
[30] Department of Astronomy, Michigan State University.
[31] Laboratory for Astronomy and Solar Physics, Goddard Space Flight Center.
[31] Institute of Physics and Astronomy, National Central University
[33] Max-Planck-Institut für Astronomie, Heidelberg.
[34] Laboratory for High Energy Astrophysics, Goddard Space Flight Center.

I. INTRODUCTION

Variability of the continuum and emission lines in active galactic nuclei (AGNs) is a well-established phenomenon (see Peterson 1988 for a review). The observed variations in the broad emission lines are apparently strongly correlated with variations in the ultraviolet and optical continua. This single fact suggests that it may be possible to determine the size and structure of the broad-line region (BLR) from the detailed response of the emission lines to the changes in the continuum flux, although it is certainly clear that there are many pitfalls that one may encounter in actual practice. Nevertheless, the possibility of extracting such fundamental information about these spatially unresolved regions has led to considerable efforts to monitor the variable spectra of AGNs. Only recently has the observational problem become sufficiently well defined that it is possible to obtain reliable results (see Netzer 1989).

In order to resolve temporally AGN continuum and emission-line behavior sufficiently well that it is possible to infer reliable structural information about the emission-line regions, an enormous amount of data is required, at least by the standards of faint-object astronomy. Recognition of this led to a large international effort to observe the Seyfert 1 galaxy NGC 5548 with the *International Ultraviolet Explorer* (*IUE*) every 4 days for an 8 month period. The results of this experiment are reported by Clavel *et al.* (1991, hereafter Paper I). It was also recognized that a concurrent ground-based program would enhance the scientific return on this considerable investment of *IUE* time (1) by extending the continuum coverage through the optical and IR, (2) by including the important Balmer series emission lines in the study, and (3) by providing both velocity resolution and signal-to-noise ratios unattainable with *IUE*. Moreover, it might be possible to achieve even better temporal resolution than planned with *IUE*, at least during limited intervals. Weather considerations made cooperation among observatories imperative to achieve reasonable temporal resolution and minimize gaps in the temporal coverage. The principal disadvantage of this approach is that the data are not extremely homogeneous or even close to regularly sampled. While this certainly introduces difficulties, these have been found to be surmountable.

In this contribution we present the ground-based optical data on NGC 5548 obtained during the period 1988 December–1989 October when this galaxy was intensely studied with *IUE*, as described in Paper I. These data, together with the ultraviolet spectra of Paper I, constitute a unique large data base for study of AGN spectral variability. In this paper we focus our attention on the primary scientific goal of this project, namely, determination of the time scale for the response of the Hβ emission line to continuum variations. Further analysis of these data will appear in future papers.

We present the optical spectroscopy and photometry obtained in this study in § II. In § III we discuss how we have constructed a homogeneous data base from these observations to produce light curves for the optical continuum and the Hβ emission line. We perform some preliminary time-series analysis in § IV, and compare the results obtained here with the results of Paper I. Our conclusions are summarized in § V.

II. OBSERVATIONS

a) *Optical Spectroscopy*

Optical spectra of NGC 5548 were obtained at many observatories as part of this campaign. A complete log of spectroscopic observations appears in Table 1. The UT date and Julian Date of each observation are given in columns (1) and (2), respectively. The column (3) entry indicates the observatory and instrument which obtained the spectrum. The projected spectrograph entrance aperture, in arcseconds, is given in column (4). For rectangular apertures, the first dimension is the slit width in the dispersion direction, and the second dimension is the slit length in the cross-dispersion direction; in the case of two-dimensional detectors (CCDs and IPCS), the second entry is the "extraction window" used. The slit position angle is given in column (5), measured eastward from north; the cross-dispersion direction runs north-south for a position angle 0°. An estimate of the seeing is given in column (6), except for the case of the Wise Observatory data, which were obtained through such large apertures that the seeing is irrelevant. The nominal spectral resolution is given in column (7), and column (8) contains the approximate wavelength range covered by the data. Finally, to aid future investigators who will make use of these data, column (9) gives a unique identifier by which the spectrum is known to the IRAF reduction system, and which is contained in the FITS file header. The first two characters ("n5") in this name identify the galaxy as NGC 5548, and the next four characters (e.g., "7509") contain the four least significant figures in the Julian Date, as in column (2). The next character gives the observatory code, as in column (3). When necessary, an additional arbitrary character is added to eliminate any remaining ambiguity.

b) *Photometry*

A program of photographic photometry was carried out with the 0.76 m telescope of the Rosemary Hill Observatory in Bronson, Florida. Photographs were obtained in three colors: *U* (Kodak 103a-O + UG-2), *B* (Kodak 103a-O + GG-385), and *V* (Kodak 103a-D + GG-495). All plates were hypersensitized, and the exposure lengths were in each case 2 minutes or less. The galaxy and comparison star measurements were made with a Cuffey Iris Astrophotometer. To suppress the starlight contribution from the host galaxy, a fixed iris corresponding to 7″ in diameter was used for all measurements. The measurements were calibrated by using four nearby comparison stars (Penston, Penston, and Sandage 1971). The results obtained in this program are summarized in Table 2.

A program of *UBVR* photoelectric photometry was also carried out with the 0.61 m Table Mountain telescope, and the results are given in Table 3. Note that the small differences between the first two sets of measurements, which are only one night apart, are undoubtedly due to the different aperture sizes used.

Broad-band photometric measurements were also obtained with a Photometrics liquid nitrogen–cooled CCD system with a Thomson 7882 chip on the 0.4 m telescope of Foggy Bottom Observatory of Colgate University. The combination of the CCD response and the blue (Mould) filter (kindly loaned by Kitt Peak National Observatory) approximates Johnson *B*. The integrated magnitudes inside a circular aperture of diameter 17″.5, centered on the nucleus of the galaxy, are given in Table 4. Star 1 from Penston, Penston, and Sandage (1971) was used as a comparison star.

III. ANALYSIS OF THE DATA

While Table 1 contains a complete log of all spectra obtained in this program, we will at this time confine our attention only to those data which cover the Hβ spectral

TABLE 1

LOG OF SPECTROSCOPIC OBSERVATIONS

UT Date (1)	Julian Date (2440000+) (2)	Code (3)	Aperture Size (4)	Aperture P.A. (5)	Seeing (") (6)	Res. (Å) (7)	Range (Å) (8)	IRAF file (9)
1988 Dec 14	7509	H	4.0 x 10.0	120.	3	5	4290 – 5100	n57530ha
1988 Dec 14	7509	H	15.0 x 10.0	120.	3	10	4290 – 5100	n57530hb
1988 Dec 14	7509	H	4.0 x 10.0	120.	3	20	3100 – 6280	n57530hc
1988 Dec 17	7512	M	2.4 x 10.0	0.	1.5	2	4750 – 5200	n57512ma
1988 Dec 17	7512	M	2.4 x 10.0	0.	1.5	2	6230 – 6800	n57512mb
1988 Dec 22	7517	A	5.0 x 7.6	90.	4–5	9	4470 – 5620	n57517a
1988 Dec 29	7524	I	4.5 x 27.2	90.	2	14	3200 – 6050	n57524ia
1988 Dec 29	7524	I	4.5 x 27.2	90.	2	14	5800 – 8400	n57524ib
1988 Dec 29	7524	I	4.5 x 27.2	90.	2	4	4600 – 5350	n57524ic
1988 Dec 30	7525	I	4.5 x 27.2	90.	3–4	14	3230 – 6100	n57525ia
1988 Dec 30	7525	I	4.5 x 27.2	90.	3–4	14	5800 – 8400	n57525ib
1989 Jan 1	7528	F	3.2 x 6.4	90.	1	5	4540 – 7050	n57528f
1989 Jan 4	7530	M	1.2 x 10.0	90.	2	4	6200 – 7000	n57530m
1989 Jan 4	7530	H	4.0 x 10.0	131.	2	5	4350 – 5150	n57530ha
1989 Jan 4	7530	H	15.0 x 10.0	131.	2	10	4350 – 5150	n57530hb
1989 Jan 6	7532	M	1.2 x 10.0	0.	1.5	4	6200 – 7000	n57532m
1989 Jan 6	7533	F	3.2 x 6.4	90.	1–2	5	4540 – 7050	n57533f
1989 Jan 8	7534	A	5.0 x 7.6	90.	2–3	9	4610 – 5580	n57534a
1989 Jan 9	7535	M	1.5 x 10.0	0.	1.0	3	6200 – 7000	n57535m
1989 Jan 9	7535	A	5.0 x 7.6	90.	2–3	9	4560 – 5710	n57535a
1989 Jan 12	7539	F	3.2 x 6.4	90.	1–2	5	4540 – 7050	n57539f
1989 Jan 13	7539	M	2.1 x 10.0	0.	2	10	4000 – 6900	n57539m
1989 Jan 16	7543	F	3.2 x 6.4	90.	1	5	4540 – 7050	n57543f
1989 Jan 20	7546	M	2.1 x 10.0	0.	3–4	10	4000 – 6900	n57546m
1989 Jan 23	7549	M	2.0 x 10.0	0.	2.5	5	3800 – 5500	n57549m
1989 Jan 30	7556	H	2.1 x 7.9	90.	2	7	4200 – 5800	n57556ha
1989 Jan 30	7556	H	7.0 x 7.9	90.	2	18	4200 – 5800	n57556hb
1989 Feb 3	7560	M	1.8 x 10.0	0.	3	3	4720 – 5670	n57560m
1989 Feb 3	7560	A	5.0 x 7.6	90.	3–4	9	4500 – 5620	n57560a
1989 Feb 3	7561	E	5.0 x 9.6	90.	5	5	4440 – 5400	n57561e
1989 Feb 6	7564	E	5.0 x 11.8	90.	3	3	4440 – 5400	n57564e
1989 Feb 7	7565	E	5.0 x 8.6	90.	2	3	4440 – 5400	n57565e
1989 Feb 9	7567	E	5.0 x 9.8	90.	3	5	4450 – 5400	n57567e
1989 Feb 10	7568	E	5.0 x 12.6	90.	3	5	4400 – 5360	n57568e
1989 Feb 12	7570	F	3.2 x 6.4	90.	1–2	5	4540 – 7050	n57570f
1989 Feb 13	7571	F	3.2 x 6.4	90.	1–2	5	4540 – 7050	n57571f
1989 Feb 14	7572	E	5.0 x 8.8	90.	2	5	4430 – 5400	n57572e
1989 Feb 15	7572	M	1.2 x 10.0	0.	2	2	6100 – 6980	n57572m
1989 Feb 16	7573	B	20.0 x 28.0	0.		10	4670 – 7020	n57573b
1989 Feb 16	7573	M	1.2 x 10.0	0.	1.5	2	4600 – 5480	n57573m
1989 Feb 16	7573	A	5.0 x 7.6	90.	2	9	4450 – 5600	n57573a
1989 Feb 17	7574	M	3.0 x 10.0	0.	1	9	4000 – 7010	n57574m
1989 Feb 17	7574	I	4.5 x 27.2	90.	2	14	3200 – 6100	n57574ia
1989 Feb 17	7574	I	4.5 x 27.2	90.	2	14	5800 – 7500	n57574ib
1989 Feb 17	7574	I	4.5 x 27.2	90.	2	4	4550 – 5300	n57574ic
1989 Feb 18	7575	M	2.0 x 10.0	0.	1.5	2	4400 – 5250	n57575ma
1989 Feb 18	7575	M	2.0 x 10.0	0.	1.5	2	6100 – 7200	n57575mb
1989 Feb 19	7576	M	2.0 x 10.0	0.	2	4	3840 – 5420	n57576m
1989 Feb 25	7582	A	5.0 x 7.6	90.	4	9	4590 – 5710	n57582a
1989 Feb 26	7583	N	4.6 x 19.2	0.	2	16	4180 – 8660	n57583n
1989 Feb 27	7584	B	20.0 x 28.0	0.		10	4600 – 7020	n57584b
1989 Mar 2	7587	M	2.0 x 10.0	90.	2	11	4230 – 7350	n57587m
1989 Mar 2	7587	F	3.2 x 6.4	90.	1–2	5	4510 – 6950	n57587f
1989 Mar 4	7589	M	2.0 x 10.0	0.	1.5	11	3830 – 7170	n57589m
1989 Mar 4	7589	A	5.0 x 7.6	90.	5	9	4460 – 5560	n57589a
1989 Mar 5	7590	L	2.0 round	–	3	3	4240 – 5060	n57590l
1989 Mar 5	7590	A	5.0 x 7.6	90.	4–5	9	4430 – 5550	n57590a
1989 Mar 5	7591	F	3.2 x 6.4	90.	2–3	5	4510 – 6950	n57591f
1989 Mar 6	7592	F	3.2 x 6.4	90.	2–3	5	4510 – 6950	n57592f
1989 Mar 7	7592	M	2.0 x 10.0	90.	1	11	3830 – 7160	n57592m
1989 Mar 7	7592	J	7.0 x 7.2	0.	2	11	3300 – 6000	n57592j
1989 Mar 7	7593	F	3.2 x 6.4	90.	1	5	4510 – 6950	n57593fa
1989 Mar 8	7593	J	7.0 x 7.2	0.	2	11	4500 – 7190	n57593j
1989 Mar 8	7593	F	3.2 x 6.4	90.	1	5	4510 – 6950	n57593fb
1989 Mar 9	7594	M	2.6 x 10.0	0.	2	2	4630 – 5500	n57594m
1989 Mar 12	7597	M	2.6 x 10.0	0.	2	2	4630 – 5500	n57597m
1989 Mar 13	7598	F	3.2 x 6.4	90.	1	5	4510 – 6950	n57598f
1989 Mar 14	7599	F	3.2 x 6.4	90.	1	5	4510 – 6950	n57599f
1989 Mar 14	7599	K	1.7 x 3.0	0.	1.5	4	4230 – 5500	n57599ka
1989 Mar 14	7599	K	1.7 x 3.0	0.	1.5	10	4550 – 7400	n57599kb
1989 Mar 15	7600	A	5.0 x 7.6	90.	2–3	9	4470 – 5600	n57600a

TABLE 1—*Continued*

UT Date (1)	Julian Date (2440000+) (2)	Code (3)	Aperture Size (4)	Aperture P.A. (5)	Seeing (") (6)	Res. (Å) (7)	Range (Å) (8)	IRAF file (9)
1989 Mar 15	7600	K	6.7 x 3.0	0.	1.5	14	4520 – 7500	n57600k
1989 Mar 16	7601	M	2.0 x 10.0	0.	1.5	2	4630 – 5500	n57601m
1989 Mar 16	7601	K	1.7 x 3.0	0.	1.5	10	4520 – 7500	n57601k
1989 Mar 21	7606	A	5.0 x 7.6	90.	2	9	4450 – 5500	n57606a
1989 Mar 21	7606	M	2.0 x 10.0	0.	4	2	4620 – 5500	n57606m
1989 Mar 28	7613	I	4.5 x 27.2	90.	3–4	14	3200 – 5860	n57613ia
1989 Mar 28	7613	I	4.5 x 27.2	90.	3–4	14	5550 – 7500	n57613ib
1989 Mar 28	7613	I	4.5 x 27.2	90.	3–4	4	4400 – 5140	n57613ic
1989 Mar 29	7614	H	4.0 x 10.0	60.	3	20	3120 – 9180	n57614h
1989 Mar 30	7615	F	3.2 x 6.4	90.	1	5	4470 – 6960	n57615f
1989 Mar 31	7616	D	8.0 x 4.0	66.9	1.5	13	3370 – 9660	n57616da
1989 Mar 31	7616	D	1.0 x 4.0	66.9	1.5	6	3370 – 9660	n57616db
1989 Apr 1	7617	F	3.2 x 6.4	90.	1	5	4520 – 7050	n57617f
1989 Apr 2	7618	F	3.2 x 6.4	90.	3	5	4520 – 7050	n57618f
1989 Apr 2	7618	A	5.0 x 7.6	90.	1.5	9	4470 – 5580	n57618a
1989 Apr 4	7620	Q	4.0 x 4.0	90.	1–2	9	3520 – 6560	n57620q
1989 Apr 4	7620	F	3.2 x 6.4	90.	2	5	4520 – 7050	n57620f
1989 Apr 4	7621	H	2.1 x 8.1	90.	3–4	7	4000 – 6500	n57621h
1989 Apr 5	7621	F	3.2 x 6.4	90.	2	5	4550 – 7050	n57621f
1989 Apr 6	7623	Q	4.0 x 4.0	90.	4–5	9	3520 – 6560	n57622q
1989 Apr 7	7623	F	3.2 x 6.4	90.	2	5	4510 – 7050	n57623f
1989 Apr 7	7623	K	2.4 x 3.0	0.	1.5	10	4760 – 7540	n57623k
1989 Apr 8	7624	F	3.2 x 6.4	90.	2	5	4510 – 7050	n57624f
1989 Apr 8	7624	K	2.4 x 3.0	0.	1.5	10	4750 – 7560	n57624k
1989 Apr 10	7626	F	3.2 x 6.4	90.	2	5	4510 – 7050	n57626f
1989 Apr 10	7626	K	2.4 x 3.0	0.	1.5	10	4760 – 7550	n57626k
1989 Apr 11	7627	F	3.2 x 6.4	90.	2	5	4510 – 7050	n57627f
1989 Apr 11	7627	A	5.0 x 7.6	90.	4–5	9	4520 – 5640	n57627a
1989 Apr 12	7628	H	2.1 x 7.9	90.	2.5	7	4200 – 5820	n57628ha
1989 Apr 12	7628	H	7.0 x 7.9	90.	2.5	18	4200 – 5820	n57628hb
1989 Apr 13	7629	E	5.0 x 11.2	90.	3	4	4620 – 5270	n57629e
1989 Apr 15	7631	P	8.0 x 9.0	90.	2	20	4400 – 7100	n57631p
1989 Apr 15	7631	N	4.6 x 19.2	0.	3	18	4300 – 8660	n57631n
1989 Apr 16	7632	P	8.0 x 9.0	90.	2–3	20	4400 – 7100	n57632p
1989 Apr 26	7642	A	5.0 x 7.6	90.	4–5	9	4490 – 5620	n57642a
1989 Apr 27	7643	F	3.2 x 6.4	90.	2	5	4550 – 7050	n57643f
1989 Apr 27	7643	H	4.0 x 10.0	60.	2	20	3110 – 9180	n57643h
1989 Apr 27	7644	M	2.1 x 10.0	0.	5	2	4750 – 5310	n57644m
1989 Apr 28	7644	B	20.0 x 28.0	0.		10	4620 – 7010	n57644b
1989 Apr 28	7644	F	3.2 x 6.4	90.	2	5	4540 – 7050	n57644f
1989 Apr 29	7645	I	4.5 x 27.2	60.	3–4	14	3200 – 6000	n57645ia
1989 Apr 29	7645	I	4.5 x 27.2	60.	3–4	14	5500 – 7500	n57645ib
1989 Apr 29	7645	I	4.5 x 27.2	60.	3–4	4	4370 – 5150	n57645ic
1989 May 1	7648	M	2.1 x 10.0	0.	3	2	4750 – 5320	n57648m
1989 May 3	7649	A	5.0 x 7.6	90.	3–5	9	4500 – 5640	n57649a
1989 May 3	7649	P	8.0 x 9.0	90.	2–3	20	4400 – 7100	n57649p
1989 May 4	7650	E	5.0 x 11.0	90.	2	2	4810 – 5130	n57650e
1989 May 7	7653	A	5.0 x 7.6	90.	2–3	9	4450 – 5550	n57653aa
1989 May 7	7653	A	1.0 x 7.6	90.	2–3	4	4450 – 5550	n57653ab
1989 May 8	7654	A	5.0 x 7.6	90.	2–3	9	4450 – 5610	n57654aa
1989 May 8	7654	A	1.0 x 7.6	90.	2–3	4	4450 – 5610	n57654ab
1989 May 8	7654	E	5.0 x 13.1	90.	3	2	4790 – 5110	n57654e
1989 May 8	7654	F	3.2 x 6.4	90.	1–2	5	4540 – 7060	n57654f
1989 May 9	7655	Q	4.0 x 4.0	90.	1–2	9	3520 – 6560	n57655q
1989 May 9	7655	A	5.0 x 7.6	90.	4–5	15	3400 – 6000	n57655ab
1989 May 9	7655	A	1.0 x 7.6	90.	4–5	11	3400 – 6000	n57655aa
1989 May 9	7656	M	2.4 x 10.0	0.	2	2	4730 – 5300	n57656m
1989 May 10	7656	F	3.2 x 6.4	90.	1–2	5	4540 – 7060	n57656f
1989 May 11	7657	A	5.0 x 7.6	90.	3–4	9	4470 – 5620	n57657aa
1989 May 11	7657	A	1.0 x 7.6	90.	3–4	4	4470 – 5620	n57657ab
1989 May 12	7658	H	2.1 x 8.6	90.	1.5	7	4210 – 5810	n57658ha
1989 May 12	7658	H	7.0 x 11.9	90.	1.5	18	4210 – 5810	n57658hb
1989 May 14	7660	I	4.5 x 27.2	130.	1.5–3	14	3200 – 6070	n57660ia
1989 May 14	7660	I	4.5 x 27.2	130.	1.5–3	14	5740 – 7500	n57660ib
1989 May 14	7660	I	4.5 x 27.2	130.	1.5–3	4	4350 – 5120	n57660ic
1989 May 15	7661	B	20.0 x 28.0	0.		10	4600 – 6980	n57661b
1989 May 16	7663	M	2.0 x 10.0	0.	2	11	3760 – 7080	n57663ma
1989 May 16	7663	M	3.0 x 10.0	0.	2	15	3760 – 7080	n57663mb

TABLE 1—*Continued*

UT Date (1)	Julian Date (2440000+) (2)	Code (3)	Aperture Size (4)	P.A. (5)	Seeing (") (6)	Res. (Å) (7)	Range (Å) (8)	IRAF file (9)
1989 May 16	7663	M	4.0 x 10.0	0.	2	21	3760 – 7080	n57663mc
1989 May 16	7663	M	2.0 x 10.0	90.	2	11	3760 – 7080	n57663md
1989 May 16	7663	M	3.0 x 10.0	90.	2	15	3760 – 7080	n57663me
1989 May 19	7665	G	7.0 round	–	2–3	8	4000 – 6540	n57665g
1989 May 21	7668	M	2.1 x 10.0	0	3–4	2	4750 – 5310	n57668ma
1989 May 21	7668	M	2.1 x 10.0	0	3–4	3	6490 – 6690	n57668mb
1989 May 27	7673	F	3.2 x 6.4	90.	1	5	4140 – 7050	n57673f
1989 May 28	7674	F	3.2 x 6.4	90.	1	5	4140 – 7050	n57674f
1989 May 29	7675	D	1.0 x 7.0	61.	1–1.3	2	4850 – 5280	n57675da
1989 May 29	7675	D	1.0 x 7.0	61.	1–1.3	2	6460 – 7100	n57675db
1989 May 30	7676	D	1.0 x 7.0	61.	1–1.3	2	4850 – 5280	n57676da
1989 May 30	7676	D	1.0 x 7.0	61.	1–1.3	2	6450 – 7100	n57676db
1989 May 31	7678	L	2.0 round	–	5	3	4100 – 5080	n57678l
1989 Jun 1	7678	A	5.0 x 7.6	90.	2–3	9	4450 – 5400	n57678a
1989 Jun 1	7678	F	3.2 x 6.4	90.	1	5	4510 – 7060	n57678f
1989 Jun 1	7679	L	2.0 round	–	4	3	4110 – 5080	n57679l
1989 Jun 2	7679	F	3.2 x 6.4	90.	1	5	4510 – 7060	n57679f
1989 Jun 2	7680	L	2.0 round	–	3	3	4180 – 5070	n57680l
1989 Jun 3	7680	F	3.2 x 6.4	90.	1.5	5	4510 – 7060	n57680f
1989 Jun 3	7680	E	2.0 x 12.0	90.	2	2	4790 – 5110	n57680e
1989 Jun 4	7681	F	3.2 x 6.4	90.	1.5	5	4540 – 7060	n57681f
1989 Jun 4	7681	E	5.0 x 12.7	90.	4	2	4830 – 5150	n57681e
1989 Jun 5	7682	F	3.2 x 6.4	90.	1.5	5	4550 – 7050	n57682f
1989 Jun 5	7682	E	5.0 x 18.6	90.	3	2	4830 – 5150	n57682e
1989 Jun 6	7683	F	3.2 x 6.4	90.	1.5	5	4550 – 7050	n57683f
1989 Jun 7	7684	F	3.2 x 6.4	90.	1.5	5	4550 – 7050	n57684f
1989 Jun 8	7685	F	3.2 x 6.4	90.	1.5	5	4550 – 7050	n57685f
1989 Jun 8	7686	M	2.1 x 10.0	90	2	2	4250 – 4800	n57686ma
1989 Jun 8	7686	M	2.1 x 10.0	90	2	3	6310 – 6810	n57686mb
1989 Jun 9	7686	F	3.2 x 6.4	90.	1.5	5	4550 – 7050	n57686f
1989 Jun 9	7687	C	1.5 x 6.0	0.	1.2	4	3330 – 7320	n57687c
1989 Jun 22	7699	N	8.8 x 12.0	0.	2	15	4300 – 6870	n57699n
1989 Jun 23	7700	N	8.8 x 12.0	0.	3	10	4320 – 5970	n57700n
1989 Jun 24	7701	N	8.8 x 9.6	0.	3	10	4320 – 5970	n57701n
1989 Jun 25	7702	K	1.7 x 3.0	0.	1.5	10	4360 – 7040	n57702k
1989 Jun 26	7703	I	4.5 x 27.2	90.	2–3	14	3200 – 5460	n57703ia
1989 Jun 26	7703	I	4.5 x 27.2	90.	2–3	14	5700 – 8240	n57703ib
1989 Jun 26	7703	K	1.7 x 3.0	0.	1.5	10	4570 – 7500	n57703k
1989 Jun 27	7704	I	4.5 x 27.2	90.	2	4	4350 – 5060	n57704i
1989 Jun 28	7705	F	3.2 x 6.4	90.	1	5	4550 – 7050	n57705f
1989 Jun 29	7706	K	1.7 x 3.0	0.	1.5	4	5950 – 7250	n57706k
1989 Jun 30	7707	F	3.2 x 6.4	90.	1	5	4550 – 7050	n57707f
1989 Jul 1	7708	F	3.2 x 6.4	90.	3	5	4550 – 7050	n57708f
1989 Jul 1	7708	O	1.9 x 4.7	90.	1.5–2	4	6330 – 7340	n57708o
1989 Jul 2	7709	F	3.2 x 6.4	90.	1	5	4550 – 7050	n57709f
1989 Jul 3	7710	F	3.2 x 6.4	90.	1	5	4550 – 7050	n57710f
1989 Jul 3	7710	O	1.9 x 4.7	90.	1.5–2	3	4550 – 5550	n57710o
1989 Jul 3	7711	L	2.0 round	–	4	3	4110 – 5060	n57711l
1989 Jul 4	7711	A	5.0 x 7.6	90.	2–3	15	3400 – 5900	n57711aa
1989 Jul 4	7711	A	1.0 x 7.6	90.	2–3	11	3400 – 5900	n57711ab
1989 Jul 5	7713	M	2.1 x 10.0	0.	3	2	4660 – 5230	n57713m
1989 Jul 8	7715	F	3.2 x 6.4	90.	1	5	4550 – 7050	n57715f
1989 Jul 9	7716	H	4.0 x 10.0	61.	4	20	3050 – 9150	n57716h
1989 Jul 12	7719	A	5.0 x 7.6	90.	3–4	15	4200 – 6820	n57719aa
1989 Jul 12	7719	A	1.0 x 7.6	90.	3–4	11	4200 – 6820	n57719ab
1989 Jul 18	7725	A	5.0 x 7.6	90.	4–5	15	3550 – 6180	n57725aa
1989 Jul 18	7725	A	1.0 x 7.6	90.	4–5	11	3550 – 6180	n57725ab
1989 Jul 21	7728	N	8.8 x 12.0	0.	2–3	15	4350 – 7060	n57728n
1989 Jul 23	7730	N	8.8 x 16.8	0.	2–3	15	4420 – 7050	n57730n
1989 Jul 29	7736	H	3.0 x 6.6	62.	1.5	3	4570 – 5380	n57736ha
1989 Jul 29	7736	H	3.0 x 6.6	62.	1.5	3	3770 – 4580	n57736hb
1989 Aug 2	7741	L	2.0 round	–	3	3	4150 – 5070	n57741l
1989 Aug 3	7742	C	1.5 x 6.0	72.1	1	4	3100 – 7070	n57742c
1989 Aug 9	7748	C	1.5 x 6.0	75.4	$\leq$0.8	4	3200 – 7380	n57748c
1989 Aug 10	7749	M	1.5 x 10.0	0.	1.5	4	4480 – 5600	n57749m
1989 Aug 15	7754	M	2.1 x 10.0	0.	1.5	2	4710 – 5280	n57754m
1989 Aug 18	7757	M	2.0 x 10.0	0.	2	11	3870 – 7210	n57757m
1989 Aug 19	7758	M	2.0 x 10.0	0.	2	11	3870 – 7210	n57758m
1989 Aug 20	7759	M	1.0 x 10.0	0.	1	2	4410 – 5290	n57759m

TABLE 1—*Continued*

UT Date (1)	Julian Date (2440000+) (2)	Code (3)	Aperture Size (4)	Aperture P.A. (5)	Seeing (") (6)	Res. (Å) (7)	Range (Å) (8)	IRAF file (9)
1989 Aug 26	7765	M	1.0 x 10.0	0.	1	2	4400 – 5270	n57765m
1989 Aug 28	7766	I	4.5 x 27.2	90.	3	14	3200 – 6040	n57766ia
1989 Aug 28	7766	I	4.5 x 27.2	90.	3	14	5700 – 8400	n57766ib
1989 Aug 28	7766	I	4.5 x 27.2	90.	3	4	4350 – 5130	n57766ic
1989 Aug 28	7766	N	8.8 x 16.0	0.	2–3	10	4300 – 6000	n57766n
1989 Aug 28	7767	M	2.0 x 10.0	0.	2–3	2	4390 – 5270	n57767m
1989 Aug 29	7767	I	4.5 x 27.2	90.	3	14	3200 – 6060	n57767ia
1989 Aug 29	7767	I	4.5 x 27.2	90.	3	14	5700 – 8400	n57767ib
1989 Aug 29	7767	I	4.5 x 27.2	90.	3	4	4350 – 5120	n57767ic
1989 Sep 8	7777	H	4.0 x 10.0	61.	2	10	3400 – 6310	n57777h
1989 Sep 9	7778	I	4.5 x 27.2	90.	3	14	3200 – 6000	n57778ia
1989 Sep 9	7778	I	4.5 x 27.2	90.	3	14	5720 – 8420	n57778ib
1989 Sep 9	7778	I	4.5 x 27.2	90.	3	4	4350 – 5130	n57778ic
1989 Sep 9	7778	A	5.0 x 7.6	90.	2–3	11	3400 – 5890	n57778a
1989 Sep 10	7779	I	4.5 x 27.2	90.	1.5–2	14	3200 – 6050	n57779ia
1989 Sep 10	7779	I	4.5 x 27.2	90.	1.5–2	14	5700 – 8420	n57779ib
1989 Sep 28	7797	H	4.0 x 10.0	59.	3–4	10	3400 – 6310	n57797h
1989 Oct 10	7809	H	4.0 x 10.0	60.	1–2	10	4700 – 6310	n57809h

NOTE.—Codes for Data origin (col. [3]) are as follows:

A 1.8 m Perkins telescope + Ohio State CCD spectrograph
B 1.0 m Wise telescope + CCD spectrograph
C 2.5 m Isaac Newton telescope + IPCS
D 5.0 m Hale telescope + double spectrograph
E 1.8 m DAO telescope + CCD spectrograph
F 1.6 m Mount Hopkins telescope + Reticon scanner
G 1.8 m Perkins telescope + Ohio State IDS
H 3.0 m Shane telescope + UV Schmidt spectrograph
I 2.3 m Steward telescope + CCD spectrograph
J 2.7 m McDonald telescope + Cassegrain grating spectrograph
K 2.4 m MDM telescope + Mark IIIb CCD spectrograph
L 6.0 m Special Astrophysical Observatory telescope + TV scanner
M 3.5 m and 2.2 m Calar Alto Observatory + CCD spectrographs
N 1.0 m Nickel telescope, Lick Observatory + CCD spectrograph
O 2.1 m telescope, Kitt Peak National Observatory + Gold Camera
P 2.1 m McDonald telescope + electronic spectrograph + CCD
Q 2.7 m McDonald telescope + IDS

TABLE 2

PHOTOGRAPHIC PHOTOMETRY

UT Date (1)	Julian Date (2,440,000+) (2)	*U* (3)	*B* (4)	*V* (5)
1988 Dec 14	7509	13.51 ± 0.03	14.11 ± 0.09	13.84 ± 0.11
1988 Dec 18	7513	13.17 ± 0.04	14.14 ± 0.14	13.71 ± 0.07
1989 Jan 27	7553	...	13.93 ± 0.08	...
1989 Mar 11	7596	13.46 ± 0.07	14.10 ± 0.12	13.78 ± 0.09
1989 Mar 12	7597	13.55 ± 0.11	13.94 ± 0.13	13.82 ± 0.27
1989 Mar 29	7614	13.23 ± 0.14	13.87 ± 0.08	13.75 ± 0.17
1989 Apr 1	7617	...	13.89 ± 0.09	...
1989 Apr 17	7633	12.76 ± 0.28	13.68 ± 0.10	13.48 ± 0.10
1989 Apr 25	7641	...	13.79 ± 0.07	...
1989 Apr 29	7645	...	13.95 ± 0.05	...
1989 May 3	7649	12.96 ± 0.05	13.90 ± 0.09	13.63 ± 0.15
1989 May 7	7653	13.03 ± 0.07	13.98 ± 0.06	13.71 ± 0.15
1989 May 13	7659	...	13.91 ± 0.08	...
1989 May 16	7662	...	13.76 ± 0.13	...
1989 May 23	7669	13.49 ± 0.05	13.93 ± 021	13.42 ± 0.06
1989 May 27	7673	...	13.84 ± 0.18	...
1989 Jul 26	7733	...	14.56 ± 0.24	13.75 ± 0.27

TABLE 3

PHOTOELECTRIC PHOTOMETRY

UT Date (1)	Julian Date (2,440,000+) (2)	Aperture (3)	U (4)	B (5)	V (6)	R (7)
1989 Apr 6	7622	20″	...	13.64 ± 0.01	13.18 ± 0.01	13.17 ± 0.01
1989 Apr 7	7623	16	...	13.78 ± 0.04	13.33 ± 0.02	13.30 ± 0.02
1989 Apr 8	7624	16	...	13.73 ± 0.07	13.29 ± 0.01	13.27 ± 0.01
1989 Apr 9	7625	16	...	13.75 ± 0.02	13.30 ± 0.01	13.28 ± 0.01
1989 Apr 10	7626	16	...	13.76 ± 0.03	13.32 ± 0.02	13.30 ± 0.02
1989 Jun 10	7687	16	13.25 ± 0.05	14.13 ± 0.04	13.50 ± 0.02	13.47 ± 0.04
1989 Jun 11	7688	16	13.30 ± 0.08	14.18 ± 0.03	13.55 ± 0.02	13.50 ± 0.04
1989 Jul 1	7708	16	13.18 ± 0.04	14.11 ± 0.03	13.48 ± 0.02	13.42 ± 0.03

region, since these are by far the most numerous data, as well as the easiest to calibrate.

a) *Absolute Calibration of the Spectra*

Absolute flux calibration of optical spectra of variable AGNs can be accomplished reliably by noting that the flux in the narrow emission lines is constant over the time scales of interest in this study. The large spatial extent of the narrow-line region (NLR) and the low electron density (which implies a very long recombination time) tend to damp out the effect of any short-term variability of the ionizing continuum. We thus use the strong, narrow [O III] λ5007 as an internal flux standard for variability studies. We note that the relative spectral energy distribution in the observed spectrum is calibrated by referencing the data to observations of a known standard star, usually Feige 98 (Stone 1977) in the case of these observations, but the absolute calibration of the spectrum is given by multiplying the data by a constant factor to give the correct [O III] λ5007 flux.

TABLE 4

CCD PHOTOMETRY

UT Date (1)	Julian Date (2,440,000+) (2)	B (3)
1989 Mar 8	7593	14.154 ± 0.044
1989 Mar 27	7612	13.901 ± 0.016
1989 Apr 9	7625	13.810 ± 0.012
1989 Apr 17	7633	13.853 ± 0.015
1989 Apr 22	7638	13.834 ± 0.021
1989 Apr 24	7640	13.792 ± 0.007
1989 May 18	7664	13.886 ± 0.020
1989 May 26	7672	13.885 ± 0.072
1989 May 27	7673	13.943 ± 0.006
1989 May 29	7675	13.952 ± 0.007
1989 Jun 3	7680	13.950 ± 0.012
1989 Jun 12	7689	14.072 ± 0.014
1989 Jun 18	7695	14.021 ± 0.032
1989 Jun 29	7706	14.048 ± 0.022
1989 Jul 3	7710	14.007 ± 0.018
1989 Jul 7	7714	13.980 ± 0.009
1989 Jul 9	7716	13.978 ± 0.015
1989 Jul 12	7719	13.966 ± 0.013
1989 Jul 19	7726	14.040 ± 0.040
1989 Jul 24	7731	14.110 ± 0.030
1989 Jul 31	7738	14.270 ± 0.020
1989 Aug 6	7744	14.270 ± 0.020
1989 Aug 7	7745	14.220 ± 0.024
1989 Aug 9	7747	14.170 ± 0.040
1989 Aug 25	7763	14.164 ± 0.010
1989 Sep 2	7771	14.101 ± 0.019
1989 Sep 3	7772	14.024 ± 0.017

The absolute flux in the [O III] λ5007 line is obtained by averaging measurements made through large spectrograph entrance apertures on photometric nights. The data from Table 1 which meet these criteria are listed in Table 5.

It is worth noting that one set of data, that from Wise Observatory, was treated in a slightly different fashion. These data were obtained with a very long slit instrument which was rotated to accept the light from both the target galaxy and star 1 of Penston, Penston, and Sandage (1971). This can be an especially accurate means of flux calibration (Maoz *et al.* 1990). The data can then be placed on an absolute flux scale once the flux of the nearby star is accurately measured. All [O III] λ5007 flux measurements from the Wise Observatory spectra are thus averaged together in Table 5, since they constitute a single determination which, as can be seen, is in excellent agreement with the mean of the other measurements.

b) *Spectral Measurements*

As we will discuss below, each set of data was treated separately to minimize aperture effects. Each set of data, as designated by the individual codes in column (3) of Table 1, was treated as being homogeneous. By making the well-justified

TABLE 5

ABSOLUTE CALIBRATION OF [O III] λ5007

F([O III] λ5007) (10^{-13} ergs cm^{-2} s^{-1}) (1)	Aperture Size (2)	Source/File Name (3)
6.06	4″.5 × 27″.2	n57524ia
5.51	4.5 × 27.2	n57524ic
6.01	4.5 × 27.2	n57525ia
5.71	4.0 × 10.0	n57530ha
5.60	15.0 × 10.0	n57530hb
5.45	7.0 × 7.9	n57556hb
5.36	4.5 × 27.2	n57574ia
5.49	4.5 × 27.2	n57574ib
5.19	7.0 × 7.2	n57592j
5.85	5.0 × 7.6	n57606a
6.11	4.0 × 10.0	n57614h
5.22	4.0 × 10.0	n57643h
5.28	7.0 × 11.9	n7658hb
5.48	4.5 × 27.2	n57703ia
5.77	4.0 × 10.0	n57716h
5.52	4.5 × 27.2	n57778ia
5.44	4.5 × 27.2	n57778ic
5.50	4.5 × 27.2	n57779ia
5.53 ± 0.31[a]	20.0 × 28.0	...
5.58 ± 0.27[b]	...	...

[a] Mean of Wise spectra (see text).
[b] Mean value (adopted absolute flux).

(Table 5) assumption that the narrow-line flux F([O III] λ5007) is constant over the time scales of interest, variability in the continuum and the Hβ emission line can be discerned by measuring the ratios F_λ/F([O III] λ5007) and F(Hβ)/F([O III] λ5007), respectively, where F_λ refers to the continuum flux at some specified wavelength and F(Hβ) is the integrated flux in the Hβ line. Since we are interested only in the *variability* of the continuum and emission lines, the details of how the measurements are done are less important than doing them in a systematic way. We therefore opted to make the simplest possible measurement of the Hβ flux by interpolating a continuum underneath the broad Hβ feature from the local depression between Hβ and the He II λ4686 + Fe II λ4570 blend (i.e., at about 4785 Å in the rest-frame of NGC 5548) to the local minimum between [O III] λ5007 and the Fe II λ5250 blend (at $\sim$5100 Å). The Hβ flux is taken to be the total flux above this continuum between the shortward limit and just shortward of [O III] λ4959 (i.e., $\sim$4940 Å). We then take as the continuum measurement the value of the interpolated continuum underneath Hβ at a point halfway between the integration limits, i.e., at about 4870 Å. The continuum and integration limits are shown graphically for a sample spectrum in Figure 1.

Strictly speaking, neither of the measured quantities is very accurate on an absolute scale, although these measurements have the great virtue of being unambiguous and highly repeatable. The continuum measurement is affected by the considerable starlight contribution and heavily blended emission features. The Hβ measurement includes the narrow-line component [$\sim$0.1F([O III] λ5007)] and contaminating emission from blends of Fe II. A careful deconvolution of the Fe II emission indicates that removal of these latter contaminants would decrease our measurements of F(Hβ) systematically by about 5%. We note that repeated measurements using slightly different continua and integration limits affect the measurements typically at about the 2% level. The uncertainties in the measured quantities will be discussed in more detail in the next section.

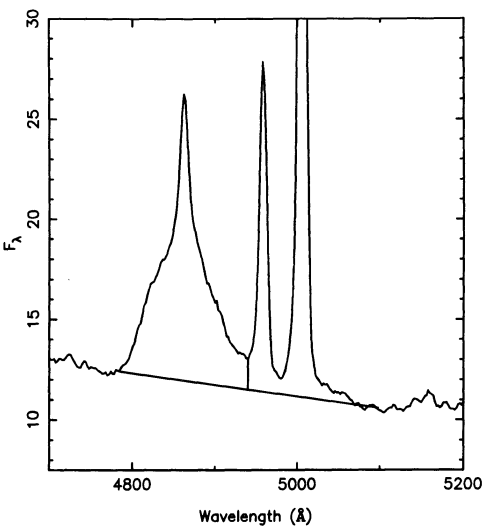

FIG. 1.—Expanded view of the spectral region near Hβ shown to illustrate how the spectral features are measured. A straight pseudocontinuum is drawn from the local minima just shortward and just longward of the Hβ + [O III] blend. The Hβ flux is taken to be the integral above this line from the shortward limit to the vertical line immediately shortward of [O III] λ4959, and the continuum flux F_λ(4870 Å) is the pseudocontinuum value at 4870 Å.

The measured values of F_λ(4870 Å)/F([O III] λ5007) and F(Hβ)/F([O III] λ5007), grouped into data sets which are regarded as homogeneous, are given in Table 6. Column (5) of Table 6 points out a few cases which merit special attention. First, we note that the Wise Observatory spectra are already on a reliable flux scale. Therefore, the ratios given in columns (2) and (3) of Table 6 for the Wise Observatory data are computed using the adopted mean value for F([O III] λ5007) given in Table 5. In a few cases we were unable to use [O III] λ5007 for flux calibration, either because it was saturated, clearly corrupted by an instrumental effect or cosmic-ray or other non-Poissonian source of noise, or in some cases because it lies beyond the long-wavelength cutoff of the spectrum. In these cases we used [O III] λ4959 as a flux standard, and inferred a value for F([O III] λ5007) based on the mean value of the F([O III] λ5007)/F([O III] λ4959) flux ratio measured from other spectra within the same set (note that blending and resolution effects tend to result in departures of F([O III] λ5007)/F([O III] λ4959) from its theoretical value of 2.96). In cases where the longward point we use for defining the continuum lies off the spectrum, we extrapolated the continuum beyond the limit of the spectrum by using other spectra taken within one or two days as a guide. Finally, in some of the low-resolution spectra, [O III] $\lambda\lambda$4959, 5007 are very heavily blended. In these spectra, both lines were measured together and F([O III] λ5007) was taken to be 75% of the total flux in the blend.

c) *Intercalibration of the Data*

The basic problem with using the [O III] λ5007 flux to calibrate spectra internally is that, in contrast to the pointlike BLR and nonstellar continuum source, the NLR is sometimes partially spatially resolved. In the case of NGC 5548, Wilson *et al.* (1989) show that narrow-line emission is detectable as far as $\sim$15″ from the nucleus. This means that the amount of NLR flux that is detected is a function of the size of the spectrograph entrance aperture. The problem is exacerbated by changes in seeing, since the observed surface brightness profile of the NLR is functionally different from the point-spread function (representing the BLR and nuclear continuum source), and the ratio of the integrals of these distributions over the aperture fluctuates most radically with seeing changes when the aperture size and the NLR size are comparable. Thus, the different aperture geometries used in these observations introduce systematic differences among the various data sets, and variations due to seeing contribute substantially to the uncertainties. Furthermore, the starlight from the host galaxy in NGC 5548 contributes substantially to the total continuum observed through the apertures used in this study, and clearly the amount of detected starlight is a strong function of spectrograph entrance aperture.

We implicitly assume that each of the individual data sets can be treated as internally homogeneous and that the differences between the data sets are attributable to aperture effects. The justification for this is twofold: (1) The larger individual data sets *all* show the same pattern of variability as seen in the *IUE* data of Paper I, and (2) if we consider the data sets which are the most similar in terms of spectrograph entrance aperture, spectral resolution, and signal-to-noise ratio, the differences between the measured values of F_λ (4870 Å)/F([O III] λ5007) and F(Hβ)/F([O III] λ5007) are very slight. To illustrate the latter point, *unadjusted* measurements of F_λ(4870 Å) and F(Hβ) from the 1.8 m Perkins telescope (sets A and G), the

TABLE 6

MEASUREMENTS OF SPECTRA

Julian Date (2440000+) (1)	$\frac{100F_\lambda(4870\text{Å})}{F([\text{O III}]\ \lambda5007)}$ (2)	$\frac{F(\text{H}\beta)}{F([\text{O III}]\ \lambda5007)}$ (3)	IRAF file (4)	Notes (5)
A — Ohio State CCD				
7517	1.98	1.44	n57515a	
7534	2.06	1.48	n57534a	
7535	2.10	1.50	n57535a	
7560	1.79	1.63	n57560a	
7573	1.70	1.60	n57573a	
7582	1.56	1.44	n57582a	
7589	1.83	1.42	n57589a	
7590	1.87	1.41	n57590a	
7600	2.00	1.23	n57600a	
7606	2.09	1.39	n57606a	
7618	2.30	1.46	n57618a	
7627	2.40	1.66	n57627a	
7642	2.50	1.74	n57642a	
7649	2.36	1.77	n57649a	
7653	2.36	1.80	n57653aa	
7654	2.35	1.74	n57654aa	
7655	2.32	1.78	n57655ab	
7657	2.28	1.79	n57657aa	
7678	1.98	1.67	n57678a	
7711	2.07	1.57	n57711aa	
7719	2.03	1.56	n57719aa	
7725	1.97	1.69	n57725aa	
7778	2.02	1.42	n57778a	
B — Wise Observatory CCD				
7573	2.73	1.59	n57573b	A
7584	2.73	1.38	n57584b	A
7644	3.45	1.70	n57644b	A
7661	3.26	1.70	n57661b	A
C — INT IPCS				
7687	1.84	1.54	n57687c	B
7742	1.24	1.53	n57742c	
7748	1.38	1.59	n57748c	
D — Palomar Double Spectrograph				
7616	1.98	1.67	n57616db	B
7675	1.54	1.96	n57675da	C
7676	1.62	1.85	n57676da	C
E — DAO CCD				
7561	1.95	1.70	n57561e	
7564	1.92	1.64	n57564e	
7565	1.93	1.69	n57565e	
7567	1.89	1.61	n57567e	
7568	1.84	1.52	n57568e	
7572	1.72	1.59	n57572e	
7629	2.37	1.51	n57629e	
7650	2.36	1.87	n57650e	C
7654	2.46	1.85	n57654e	C
7681	1.94	1.67	n57681e	C
7682	2.12	1.67	n57682e	C
F — SAO Reticon				
7528	1.72	1.60	n57528f	
7533	1.78	1.64	n57533f	
7539	1.88	1.53	n57539f	
7543	1.85	1.53	n57543f	
7570	1.56	1.77	n57570f	
7571	1.59	1.64	n57571f	
7587	1.52	1.56	n57587f	
7591	1.53	1.48	n57591f	
7592	1.69	1.54	n57592f	
7593	1.51	1.53	n57593fa	
7593	1.47	1.50	n57593fb	
7598	1.67	1.49	n57598f	
7599	1.72	1.39	n57599f	
7615	1.90	1.48	n57615f	
7617	1.98	1.63	n57617f	
7618	2.04	1.63	n57618f	
7620	2.09	1.62	n57620f	
7621	2.10	1.54	n57621f	
7623	2.03	1.79	n57623f	
7624	2.21	1.61	n57624f	
7626	2.08	1.65	n57626f	
7627	2.14	1.58	n57627f	
7643	2.17	1.86	n57643f	
7644	2.20	1.86	n57644f	
7650	2.18	1.91	n57650f	
7654	2.02	1.84	n57654f	
7656	2.07	1.95	n57656f	
7673	1.78	1.87	n57673f	
7674	1.76	1.89	n57674f	
G — Ohio State IDS				
7665	2.22	1.70	n57665g	
H1 — Lick Shane CCD (Large Aperture)				
7509	1.92	1.35	n57509hc	
7530	1.97	1.45	n57530ha	
7556	2.21	1.55	n57566hb	
7614	2.31	1.54	n57614h	
7628	2.54	1.56	n57628hb	
7643	2.34	1.73	n57643h	
7658	2.50	1.72	n57658hb	
7716	2.00	1.53	n577716h	
7777	1.86	1.37	n57777h	
7797	2.21	1.53	n57797h	
7809	2.09	1.57	n57809h	
H2 — Lick Shane CCD (Small Aperture)				
7556	1.86	1.65	n57556ha	
7621	2.50	1.72	n57621h	
7628	2.23	1.60	n57628ha	
7658	2.02	1.82	n57658ha	
7736	1.25	1.54	n57736ha	
I — Steward CCD				
7524	2.11	1.64	n57524ia	
7525	2.23	1.62	n57525ia	
7574	1.89	1.57	n57574ia	
7613	2.44	1.49	n57613ia	
7645	2.46	1.84	n57645ia	
7660	2.21	1.79	n57660ia	
7703	1.96	1.64	n57703ia	
7766	1.85	1.33	n57766ia	
7767	1.85	1.31	n57767ia	
7778	2.10	1.48	n57778ia	
7779	2.10	1.46	n57779ia	
J — McDonald 2.7m CCD				
7592	1.96	1.23	n57592j	
7593	2.00	1.27	n57593j	
K1 — Michigan CCD (Large Aperture)				
7600	1.90	1.30	n57600k	
K2 — Michigan CCD (Small Aperture)				
7599	1.62	1.34	n57599kb	
7601	1.60	1.28	n57601k	
7623	2.55	1.57	n57623k	
7624	2.40	1.65	n57624k	
7626	2.46	1.60	n57626k	
7702	1.61	1.52	n57702k	
7703	1.50	1.59	n57703k	
L — Special Astrophysical Observatory Scanner				
7590	1.73	1.58	n57590l	B,C
7678	1.88	1.68	n57678l	B,C

TABLE 6—*Continued*

Julian Date (2440000+) (1)	$100F_\lambda(4870\text{Å})/F([\text{O III}]\ \lambda5007)$ (2)	$F(\text{H}\beta)/F([\text{O III}]\ \lambda5007)$ (3)	IRAF file (4)	Notes (5)
L — Special Astrophysical Observatory Scanner (cont.)				
7679	1.75	1.74	n57679l	B,C
7680	1.60	1.94	n57680l	B,C
7711	1.96	1.62	n57711l	B,C
7741	1.10	1.55	n57741l	B
M — Calar Alto CCD				
7512	1.70	1.42	n57512ma	
7539	2.25	1.66	n57539m	B
7546	2.55	1.56	n57546m	
7549	2.11	1.60	n57549m	
7560	1.96	1.51	n57560m	
7573	1.45	1.58	n57573m	
7574	1.63	1.49	n57574m	
7575	1.46	1.50	n57575ma	
7576	1.44	1.47	n57576m	
7587	1.55	1.39	n57587m	
7589	1.44	1.36	n57589m	
7592	1.66	1.37	n57592m	
7594	1.64	1.21	n57594m	
7597	1.82	1.33	n57597m	
7601	1.81	1.30	n57601m	
7606	2.12	1.32	n57606m	
7644	2.43	1.56	n57644m	
7648	2.27	1.66	n57648m	
7652	2.06	1.77	n57652m	
7656	2.09	1.74	n57656m	
7663	2.06	1.82	n57663ma	
7668	2.00	1.67	n57668ma	
N1 — Lick Nickel CCD (Large Aperture)				
7699	2.55	1.55	n57699n	
7700	2.61	1.55	n57700n	
7701	2.64	1.57	n57701n	
7728	2.29	1.60	n57728n	
7730	2.47	1.55	n57730n	
7766	2.01	1.44	n57766n	
N2 — Lick Nickel CCD (Small Aperture)				
7583	1.82	1.43	n57583n	
7631	2.84	1.66	n57631n	
O — KPNO CCD				
7710	1.63	1.41	n57710o	
P — McDonald 2.1m CCD				
7631	2.66	1.51	n57631p	D
7632	2.50	1.48	n57632p	D
7649	2.43	1.49	n57649p	D
Q — McDonald 2.7m IDS				
7620	2.10	1.43	n57620q	
7622	2.06	1.49	n57622q	
7655	2.00	1.80	n57655q	

NOTES.—(A) Spectrum calibrated in absolute units by relative spectrophotometry (see text). Flux ratios computed using $F([\text{O III}]\ \lambda5007)$ from Table 5. (B) [O III] $\lambda5007$ unusable; calibration based on [O III] $\lambda4959$. (C) Redward continuum point off of spectrum; continuum extrapolated. (D) [O III] $\lambda\lambda4959$, 5007 strongly blended; [O III] $\lambda5007$ taken to be 0.75 of total blend flux.

large-aperture data from the 3 m Lick Shane telescope (set H1), the 2.3 m Steward telescope data (set I), the 2.7 m McDonald telescope CCD data (set J), and the single large-aperture observation from the 2.4 m MDM telescope (set K1) are shown in Figure 2.

We can make an empirical correction for these aperture effects by comparing data from different sets which are nearly contemporaneous. If we compare closely spaced measurements of $F(\text{H}\beta)/F([\text{O III}]\ \lambda5007)$ from different data sets, and assume

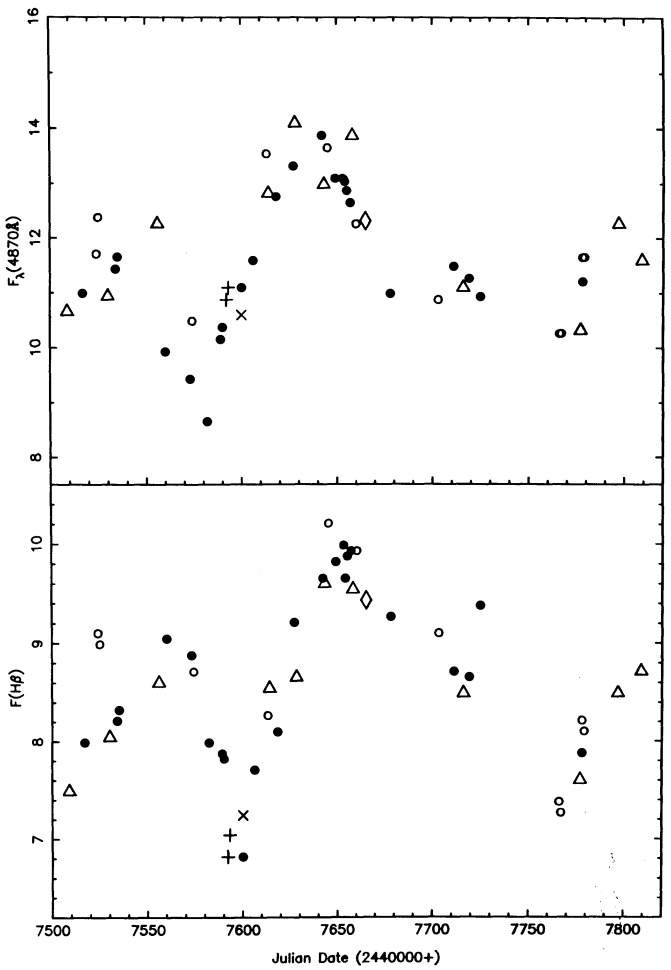

FIG. 2.—Continuum (*upper panel*) and Hβ (*lower panel*) flux measurements from high-quality spectra with similar entrance apertures. These measurements, from Table 6, are uncorrected for any aperture effects and put on an absolute flux scale by multiplying the measured flux ratios by the absolute [O III] $\lambda5007$ flux given in Table 5. *Filled circles*: set A; *diamonds*: set G; *triangles*: set H1; *open circles*: set I; *plus signs*: set J; *crosses*: set K1.

that any differences between them reflect differences in the amount of [O III] $\lambda5007$ measured, then we can compute a point-source correction factor φ which is defined by the equation

$$F(\text{H}\beta) = \varphi F_{5007}\left(\frac{F(\text{H}\beta)}{F([\text{O III}]\ \lambda5007)}\right)_{\text{obs}}, \quad (1)$$

where F_{5007} is the adopted mean [O III] $\lambda5007$ flux from Table 5 and the observed ratio is as given in Table 6. We then compute a correction for the starlight for different apertures, which enters as an additive term G, i.e.,

$$F_\lambda(4870\ \text{Å}) = \varphi F_{5007}\left(\frac{F_\lambda(4870\ \text{Å})}{F([\text{O III}]\ \lambda5007)}\right)_{\text{obs}} - G\,. \quad (2)$$

By comparing pairs of simultaneous observations from different data sets, we can determine the constants φ and G which are needed to adjust the emission-line and continuum fluxes to a common scale. Furthermore, the formal uncertainties in φ and G reflect the uncertainties in the individual data sets, so we can determine the nominal uncertainties for each data set if we assume that the errors add in quadrature.

In practice, we find that it is neither necessary nor desirable to base the intercalibration of different data sets only on observations that were made on the same day. If we require such strict simultaneity, we find that some data sets cannot be used at all because they have no points in common with other sets, and in other cases the intercalibration is very poorly determined because it is based on such a small number of points. If instead we base the comparison on pairs of points which are separated by 2 days or less, we find (*a*) that *all* of the data in Table 6 can be intercalibrated and (*b*) that the number of pairs contributing to each comparison is greatly increased, thus improving the accuracy of the result. The fundamental assumption is that no significant line or continuum variability occurs on time scales shorter than ~ 2 days. The justification for this assumption is (1) that the homogeneous *IUE* data from Paper I show no evidence for significant short-term variations and (2) that relaxing the simultaneity requirement does not significantly change the formal uncertainties in the determination of either φ or G, which is what would happen if there were real variability on short time scales. With regard to the latter point, evidence for real variability *begins* to appear on time scales longer than about 5 days. By regarding all data obtained over any 2 day interval as simultaneous, we effectively degrade our highest achievable temporal resolution. We believe, however, that the gain in temporal *coverage* and accuracy offsets this disadvantage.

Operationally, the intercalibration procedure is carried out by comparing some of the larger data sets, and then gradually building up the calibrated base by including additional data sets. All the data are calibrated relative to data set A because these data are fairly numerous, overlap reasonably well with most of the other data sets, and were obtained through a reasonably large aperture (5″ × 7″.6). The fractional uncertainties in the continuum [$\sigma_{\rm cont}/F_\lambda(4870\ \text{Å}) \approx 0.040$] and the H$\beta$ flux [$\sigma_{\rm line}/F(\text{H}\beta) \approx 0.035$] for the similar data in Figure 2, which are all high-quality spectra obtained through large apertures, were determined by comparing all pairs of measurements separated by 2 days or less. It was also possible to assess independently the uncertainties in certain other data sets. The data from the 1.6 m Mount Hopkins telescope (set F) were sufficiently well sampled on short time scales to assess their internal accuracy reliably, and the fractional uncertainties in the continuum and the line are the same as for the data shown in Figure 2. The uncertainty in the Wise Observatory (set B) measurements ($\sigma_{\rm cont}/F_\lambda(4870\ \text{Å}) \approx 0.040$; $\sigma_{\rm line}/F(\text{H}\beta) \approx 0.050$) are taken from Netzer *et al.* (1990), and the uncertainty in the single Ohio State IDS (set G) data point (5% in each parameter) is adopted from Peterson *et al.* (1990). No correction is applied to the latter point because of an insufficient number of nearly contemporaneous observations. For most of the other data sets, it was possible to estimate the mean uncertainties in the measurements by comparing them with measurements from other sets for which the uncertainties are known and by assuming that the uncertainties for each set add in quadrature. This procedure did not work well for some of the small data sets, and in such cases we simply adopted uncertainties from the larger data sets which were most similar in terms of spectrograph entrance aperture, spectral resolution, and signal-to-noise ratio. We note that this procedure seems to give fairly consistent error estimates and calibration constants regardless of the specific order in which the data bases are combined.

The intercalibration constants we use for each data set are given in Table 7. It is important to note that (1) the point-source correction factor is always close to unity, indicating that the ratio of point-source to narrow-line flux does not vary greatly with aperture (i.e., the narrow-line surface brightness distribution is in fact rather concentrated) and (2) the extended source (starlight) correction is generally in the expected sense, i.e., positive for much larger apertures than 5″ × 7″.6 and negative for much smaller apertures. For apertures of similar size the correction factors have only a small effect.

TABLE 7

FLUX SCALE FACTORS

Data Set (1)	Point-Source Scale Factor φ (2)	Extended Source Correction G (10^{-15} ergs s^{-1} cm^{-2} Å^{-1}) (3)
A	1.000	0.000
B	1.008 ± 0.043	5.845 ± 0.695
C	0.978 ± 0.103	−0.525 ± 0.582
D	0.902 ± 0.035	−3.016 ± 0.491
E	0.988 ± 0.044	−0.048 ± 0.661
F	0.931 ± 0.045	−2.349 ± 0.371
G	1.000	0.000
H1	1.000 ± 0.051	0.135 ± 0.957
H2	0.952 ± 0.053	−1.449 ± 1.084
I	0.955 ± 0.042	0.373 ± 1.024
J	1.112 ± 0.052	1.896 ± 0.382
K1	1.013 ± 0.053	−0.446 ± 0.116
K2	0.983 ± 0.048	−1.143 ± 1.249
L	0.926 ± 0.060	−1.682 ± 0.720
M	1.040 ± 0.066	−0.748 ± 0.799
N1	0.888 ± 0.064	1.443 ± 1.105
N2	0.960 ± 0.055	1.122 ± 0.931
O	1.080 ± 0.024	−1.455 ± 0.384
P	1.154 ± 0.097	2.551 ± 0.889
Q	1.027 ± 0.052	−1.712 ± 0.687

The continuum and line measurements from Table 6 are adjusted to a common scale corresponding to measurements through a 5″ × 7″.6 spectrograph entrance aperture by using the constants of Table 7 in equations (1) and (2). The resultant values of the continuum flux $F_\lambda(4870\ \text{Å})$ and the line flux $F(\text{H}\beta)$ are given in Table 8. A final light curve is produced by computing the variance-weighted average of all the measurements obtained on a given Julian Date; this light curve is given in Table 9 and shown in Figure 3. Also shown for comparison in Figure 3 are the *B*-band photometric measurements from Tables 2, 3, and 4; we have placed these measurements on an approximate flux scale by using the relationship

$$B = -2.5 \log F_\nu - 48.60 \qquad (3)$$

(Oke and Gunn 1983), where F_ν is the flux in units of ergs s^{-1} cm^{-2} Hz^{-1}.

IV. VARIABILITY ANALYSIS

a) Characteristics of the Data Base

Table 8 gives 177 separate measurements of the optical continuum and Hβ fluxes in NGC 5548 between 1988 December 14 and 1989 October 10, a period of 301 days. By averaging measurements obtained on a given Julian Date, we produce a final light curve covering 129 independent epochs, as given in Table 9. For the purpose of time-series analysis, we exclude the final two points where the light curve is poorly sampled, which leaves 127 measurements over a 271 day period. The average interval between these observations is 3.1 days, and the median

TABLE 8

SCALED FLUX MEASUREMENTS

Julian Date (2440000+) (1)	Code (2)	F_λ(4870Å) (10^{-15} ergs s^{-1} cm^{-2} Å^{-1}) (3)	F(Hβ) (10^{-13} ergs s^{-1} cm^{-2}) (4)	Julian Date (2440000+) (1)	Code (2)	F_λ(4870Å) (10^{-15} ergs s^{-1} cm^{-2} Å^{-1}) (3)	F(Hβ) (10^{-13} ergs s^{-1} cm^{-2}) (4)
7509	H1	10.58 ± 0.42	7.53 ± 0.26	7616	D	12.98 ± 1.04	8.41 ± 0.38
7512	M	10.61 ± 0.64	8.24 ± 0.45	7617	F	12.64 ± 0.50	8.47 ± 0.30
7517	A	11.05 ± 0.44	8.03 ± 0.28	7618	A	12.83 ± 0.51	8.15 ± 0.28
7524	I	10.87 ± 0.44	8.74 ± 0.31	7618	F	12.95 ± 0.52	8.47 ± 0.30
7525	I	11.51 ± 0.46	8.63 ± 0.30	7620	F	13.21 ± 0.53	8.42 ± 0.29
7528	F	11.28 ± 0.45	8.31 ± 0.29	7620	Q	13.75 ± 1.10	8.19 ± 0.37
7530	H1	10.86 ± 0.43	8.09 ± 0.28	7621	F	13.26 ± 0.53	8.00 ± 0.28
7533	F	11.60 ± 0.46	8.52 ± 0.30	7621	H2	14.73 ± 1.18	9.14 ± 0.41
7534	A	11.49 ± 0.46	8.26 ± 0.29	7622	Q	13.52 ± 1.08	8.54 ± 0.38
7535	A	11.72 ± 0.47	8.37 ± 0.29	7623	F	12.89 ± 0.52	9.30 ± 0.32
7539	F	12.11 ± 0.49	7.95 ± 0.28	7623	K2	15.13 ± 1.59	8.61 ± 0.30
7539	M	13.81 ± 0.83	9.63 ± 0.53	7624	F	13.83 ± 0.55	8.36 ± 0.29
7543	F	11.96 ± 0.48	7.95 ± 0.28	7624	K2	14.31 ± 1.50	9.05 ± 0.32
7546	M	15.55 ± 0.93	9.05 ± 0.50	7626	F	13.15 ± 0.53	8.57 ± 0.30
7549	M	12.99 ± 0.78	9.28 ± 0.51	7626	K2	14.64 ± 1.54	8.78 ± 0.31
7556	H1	12.20 ± 0.49	8.65 ± 0.30	7627	A	13.39 ± 0.54	9.26 ± 0.32
7556	H2	11.33 ± 0.91	8.77 ± 0.39	7627	F	13.47 ± 0.54	8.21 ± 0.29
7560	A	9.99 ± 0.40	9.10 ± 0.32	7628	H1	14.04 ± 0.56	8.70 ± 0.31
7560	M	12.12 ± 0.73	8.76 ± 0.48	7628	H2	13.30 ± 1.06	8.50 ± 0.38
7561	E	10.80 ± 0.43	9.37 ± 0.33	7629	E	13.11 ± 0.52	8.32 ± 0.29
7564	E	10.63 ± 0.43	9.04 ± 0.32	7631	N2	14.09 ± 0.99	8.89 ± 0.40
7565	E	10.69 ± 0.43	9.32 ± 0.33	7631	P	14.57 ± 0.66	9.72 ± 0.73
7567	E	10.47 ± 0.42	8.88 ± 0.31	7632	P	13.54 ± 0.61	9.53 ± 0.71
7568	E	10.19 ± 0.41	8.38 ± 0.29	7642	A	13.95 ± 0.56	9.71 ± 0.34
7570	F	10.45 ± 0.42	9.19 ± 0.32	7643	F	13.62 ± 0.55	9.66 ± 0.34
7571	F	10.61 ± 0.42	8.52 ± 0.30	7643	H1	12.92 ± 0.52	9.65 ± 0.34
7572	E	9.53 ± 0.38	8.77 ± 0.31	7644	B	13.50 ± 0.00	0.54 ± 9.56
7573	A	9.49 ± 0.38	8.93 ± 0.31	7644	F	13.78 ± 0.55	9.66 ± 0.34
7573	B	9.50 ± 0.00	0.38 ± 8.94	7644	M	14.85 ± 0.89	9.05 ± 0.50
7573	M	9.16 ± 0.55	9.17 ± 0.50	7645	I	12.74 ± 0.51	9.81 ± 0.34
7574	I	9.70 ± 0.39	8.37 ± 0.29	7648	M	13.92 ± 0.83	9.63 ± 0.53
7574	M	10.21 ± 0.61	8.65 ± 0.48	7649	A	13.17 ± 0.53	9.88 ± 0.35
7575	M	9.22 ± 0.55	8.70 ± 0.48	7649	P	13.09 ± 0.59	9.59 ± 0.72
7576	M	9.10 ± 0.55	8.53 ± 0.47	7650	E	13.06 ± 0.52	10.31 ± 0.36
7582	A	8.70 ± 0.35	8.03 ± 0.28	7650	F	13.67 ± 0.55	9.92 ± 0.35
7583	N2	8.63 ± 0.60	7.66 ± 0.34	7652	M	12.70 ± 0.76	10.27 ± 0.56
7584	B	9.50 ± 0.00	0.38 ± 7.76	7653	A	13.17 ± 0.53	10.04 ± 0.35
7587	M	9.74 ± 0.58	8.07 ± 0.44	7654	A	13.11 ± 0.52	9.71 ± 0.34
7587	F	10.25 ± 0.41	8.10 ± 0.28	7654	F	12.84 ± 0.51	9.56 ± 0.34
7589	M	9.10 ± 0.55	7.89 ± 0.43	7654	E	13.61 ± 0.54	10.20 ± 0.36
7589	A	10.21 ± 0.41	7.92 ± 0.28	7655	A	12.95 ± 0.52	9.93 ± 0.35
7590	A	10.44 ± 0.42	7.87 ± 0.28	7655	Q	13.17 ± 1.05	10.31 ± 0.46
7590	L	10.62 ± 0.69	8.16 ± 0.45	7656	F	13.10 ± 0.52	10.13 ± 0.35
7591	F	10.30 ± 0.41	7.69 ± 0.27	7656	M	12.88 ± 0.77	10.10 ± 0.56
7592	J	10.27 ± 0.41	7.63 ± 0.27	7657	A	12.72 ± 0.51	9.99 ± 0.35
7592	M	10.38 ± 0.62	7.95 ± 0.44	7658	H1	13.81 ± 0.55	9.60 ± 0.34
7592	F	11.13 ± 0.44	8.00 ± 0.28	7658	H2	12.18 ± 0.97	9.67 ± 0.44
7593	F	10.19 ± 0.41	7.95 ± 0.28	7660	I	11.40 ± 0.46	9.54 ± 0.33
7593	J	10.51 ± 0.42	7.88 ± 0.28	7661	B	12.40 ± 0.02	0.50 ± 9.56
7594	M	10.27 ± 0.62	7.02 ± 0.39	7663	M	12.70 ± 0.76	10.56 ± 0.58
7594	F	9.99 ± 0.40	7.79 ± 0.27	7665	G	12.39 ± 0.50	9.49 ± 0.33
7597	M	11.31 ± 0.68	7.72 ± 0.42	7668	M	12.35 ± 0.74	9.69 ± 0.53
7598	F	11.02 ± 0.44	7.74 ± 0.27	7673	F	11.60 ± 0.46	9.72 ± 0.34
7599	F	11.28 ± 0.45	7.22 ± 0.25	7674	F	11.49 ± 0.46	9.82 ± 0.34
7599	K2	10.03 ± 1.05	7.35 ± 0.26	7675	D	10.77 ± 0.86	9.86 ± 0.44
7600	K1	11.18 ± 0.45	7.34 ± 0.26	7676	D	11.17 ± 0.89	9.31 ± 0.42
7600	A	11.16 ± 0.45	6.86 ± 0.24	7678	F	10.92 ± 0.44	9.72 ± 0.34
7601	M	11.25 ± 0.68	7.54 ± 0.41	7678	A	11.05 ± 0.44	9.32 ± 0.33
7601	K2	9.92 ± 1.04	7.02 ± 0.25	7678	L	11.40 ± 0.74	8.68 ± 0.48
7606	M	13.05 ± 0.78	7.66 ± 0.42	7679	F	10.56 ± 0.42	9.40 ± 0.33
7606	A	11.66 ± 0.47	7.76 ± 0.27	7679	L	10.72 ± 0.70	8.99 ± 0.49
7613	I	12.63 ± 0.50	7.94 ± 0.28	7680	F	11.13 ± 0.44	9.66 ± 0.34
7614	H1	12.76 ± 0.51	8.59 ± 0.30	7680	L	9.95 ± 0.65	10.02 ± 0.55
7615	F	12.22 ± 0.49	7.69 ± 0.27	7681	E	10.74 ± 0.43	9.21 ± 0.32

TABLE 8—*Continued*

Julian Date (2440000+) (1)	Code (2)	F_λ(4870Å) (10^{-15} ergs s^{-1} cm^{-2} Å^{-1}) (3)	F(Hβ) (10^{-13} ergs s^{-1} cm^{-2}) (4)
7681	F	10.97 ± 0.44	9.35 ± 0.33
7682	E	11.74 ± 0.47	9.21 ± 0.32
7682	F	11.18 ± 0.45	8.88 ± 0.31
7683	F	11.49 ± 0.46	9.45 ± 0.33
7684	F	10.66 ± 0.43	9.09 ± 0.32
7685	F	11.28 ± 0.45	8.99 ± 0.31
7686	F	10.45 ± 0.42	9.25 ± 0.32
7687	C	10.57 ± 0.85	8.40 ± 0.38
7699	N1	11.19 ± 1.06	7.68 ± 0.46
7700	N1	11.49 ± 1.09	7.68 ± 0.46
7701	N1	11.64 ± 1.11	7.78 ± 0.47
7702	K2	9.97 ± 1.05	8.34 ± 0.29
7703	K2	9.37 ± 0.98	8.72 ± 0.31
7703	I	10.07 ± 0.40	8.74 ± 0.31
7705	F	10.04 ± 0.40	8.57 ± 0.30
7707	F	11.08 ± 0.44	8.52 ± 0.30
7708	F	11.02 ± 0.44	8.57 ± 0.30
7709	F	11.08 ± 0.44	8.52 ± 0.30
7710	F	10.92 ± 0.44	8.26 ± 0.29
7710	O	11.28 ± 0.90	8.50 ± 0.38
7711	A	11.55 ± 0.46	8.76 ± 0.31
7711	L	11.81 ± 0.77	8.37 ± 0.46
7713	M	11.08 ± 0.67	7.83 ± 0.43
7715	F	10.51 ± 0.42	8.21 ± 0.29
7716	H1	11.02 ± 0.44	8.54 ± 0.30
7719	A	11.33 ± 0.45	8.70 ± 0.31
7725	A	10.99 ± 0.44	9.43 ± 0.33
7728	N1	9.90 ± 0.94	7.93 ± 0.48
7730	N1	10.80 ± 1.03	7.68 ± 0.46
7736	H2	8.09 ± 0.65	8.18 ± 0.37
7741	L	7.37 ± 0.48	8.01 ± 0.44
7742	C	7.29 ± 0.58	8.35 ± 0.38
7748	C	8.06 ± 0.64	8.68 ± 0.39
7749	M	7.36 ± 0.44	7.54 ± 0.41
7754	M	7.13 ± 0.43	7.60 ± 0.42
7757	M	8.81 ± 0.53	7.37 ± 0.41
7758	M	10.50 ± 0.63	7.60 ± 0.42
7759	M	9.57 ± 0.57	6.73 ± 0.37
7765	M	7.83 ± 0.47	6.73 ± 0.37
7766	N1	8.52 ± 0.81	7.14 ± 0.43
7766	I	9.48 ± 0.38	7.09 ± 0.25
7767	M	8.81 ± 0.53	6.85 ± 0.38
7767	I	9.48 ± 0.38	6.98 ± 0.24
7777	H1	10.24 ± 0.41	7.64 ± 0.27
7778	I	10.82 ± 0.43	7.89 ± 0.28
7778	A	11.27 ± 0.45	7.92 ± 0.28
7779	I	10.82 ± 0.43	7.78 ± 0.27
7797	H1	12.20 ± 0.49	8.54 ± 0.30
7809	H1	11.53 ± 0.46	8.76 ± 0.31

interval is 1 day. The largest gaps in the coverage are 12 days (JD 2,447,687–JD 2,447,699) and 10 days (JD 2,447,632–JD 2,447,642 and JD 2,447,767–JD 2,447,777), and there are no other gaps longer than 7 days.

We can use the data in Table 9 to perform a final check on our error estimates by examining the ratios of all pairs of measurements separated by 2 days or less. In Table 9 there are 144 independent pairs of measurements within 2 days of one another. The dispersion about the mean (unity), divided by $2^{1/2}$, provides an estimate of the typical uncertainty in a single measurement. For the continuum, we find that the mean fractional error in a given measurement is 0.040. The average fractional uncertainty, from the quoted estimates for these same 144 measurements in Table 9, is 0.045. This implies that our error estimates are probably quite good, and perhaps overestimated on average by about 10%. Similarly, examination of the Hβ emission-line fluxes indicates that the fractional uncertainty is 0.033, compared with the value of 0.037 computed from the Table 9 entries. Again, this indicates that our errors may be very slightly overestimated.

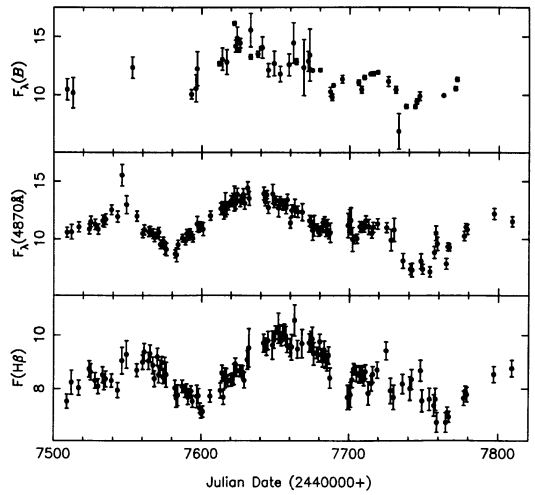

FIG. 3.—*Top panel*: photometric *B*-magnitudes from Tables 2, 3, and 4 placed on an approximate linear flux scale by using eq. (3). *Middle panel:* continuum fluxes at 4870 Å from the optical spectra, as given in Table 9. The continuum fluxes are in units of 10^{-15} ergs s^{-1} cm^{-2} Å^{-1}. *Bottom panel*: Hβ fluxes from Table 9, in units of 10^{-13} ergs s^{-1} cm^{-2}.

Inspection of Figure 3 suggests that the continuum measurement on JD 2,447,546 is anomalously high. This spectrum has been carefully inspected and remeasured, and the original data were re-reduced in an attempt to determine whether or not there might indeed be a problem with these data. We were unable to find anything obviously wrong in the original data or with the data reduction, and we have therefore kept this measurement in the data base despite our suspicion that it is too high.

b) Variability Amplitude

Significant variability was detected in both the continuum and the Hβ emission line. This is evident from inspection of the high-state and low-state spectra shown in Figure 4. The con-

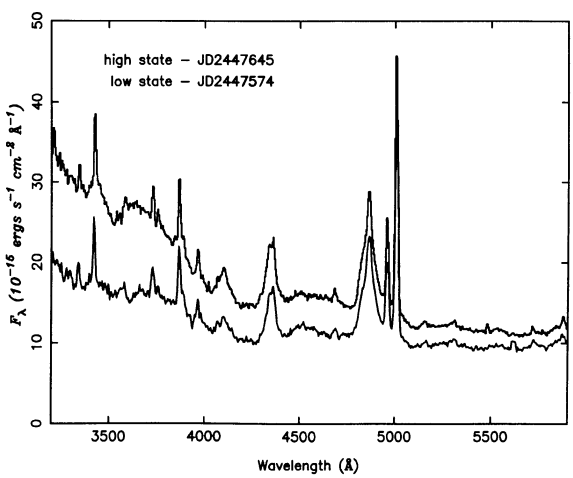

FIG. 4.—High-state and low-state optical spectra of NGC 5548. The two spectra shown here were obtained with the 2.3 m Steward Observatory telescope on Kitt Peak.

TABLE 9

OPTICAL CONTINUUM AND Hβ LIGHT CURVES

Julian Date (2440000+) (1)	F_λ(4870Å) (10^{-15} ergs s^{-1} cm^{-2} Å^{-1}) (2)	F(Hβ) (10^{-13} ergs s^{-1} cm^{-2}) (3)
7509	10.58 ± 0.42	7.53 ± 0.26
7512	10.61 ± 0.64	8.24 ± 0.45
7517	11.05 ± 0.44	8.03 ± 0.28
7524	10.87 ± 0.44	8.74 ± 0.31
7525	11.51 ± 0.46	8.63 ± 0.30
7528	11.28 ± 0.45	8.31 ± 0.29
7530	10.86 ± 0.43	8.09 ± 0.28
7533	11.60 ± 0.46	8.52 ± 0.30
7534	11.49 ± 0.46	8.26 ± 0.29
7535	11.72 ± 0.47	8.37 ± 0.29
7539	12.55 ± 0.42	8.31 ± 0.25
7543	11.96 ± 0.48	7.95 ± 0.28
7546	15.55 ± 0.93	9.05 ± 0.50
7549	12.99 ± 0.78	9.28 ± 0.51
7556	12.00 ± 0.43	8.69 ± 0.24
7560	10.48 ± 0.35	8.99 ± 0.27
7561	10.80 ± 0.43	9.37 ± 0.33
7564	10.63 ± 0.43	9.04 ± 0.32
7565	10.69 ± 0.43	9.32 ± 0.33
7567	10.47 ± 0.42	8.88 ± 0.31
7568	10.19 ± 0.41	8.38 ± 0.29
7570	10.45 ± 0.42	9.19 ± 0.32
7571	10.61 ± 0.42	8.52 ± 0.30
7572	9.53 ± 0.38	8.77 ± 0.31
7573	9.43 ± 0.24	8.98 ± 0.23
7574	9.84 ± 0.33	8.44 ± 0.25
7575	9.22 ± 0.55	8.70 ± 0.48
7576	9.10 ± 0.55	8.53 ± 0.47
7582	8.70 ± 0.35	8.03 ± 0.28
7583	8.63 ± 0.60	7.66 ± 0.34
7584	9.51 ± 0.38	7.76 ± 0.39
7587	10.08 ± 0.34	8.09 ± 0.24
7589	9.81 ± 0.33	7.91 ± 0.23
7590	10.48 ± 0.36	7.95 ± 0.23
7591	10.30 ± 0.41	7.69 ± 0.27
7592	10.61 ± 0.27	7.83 ± 0.18
7593	10.35 ± 0.29	7.91 ± 0.20
7594	10.07 ± 0.33	7.54 ± 0.22
7597	11.31 ± 0.68	7.72 ± 0.42
7598	11.02 ± 0.44	7.74 ± 0.27
7599	11.09 ± 0.41	7.28 ± 0.18
7600	11.17 ± 0.32	7.09 ± 0.18
7601	10.86 ± 0.57	7.16 ± 0.21
7606	12.03 ± 0.40	7.73 ± 0.23
7613	12.63 ± 0.50	7.94 ± 0.28
7614	12.76 ± 0.51	8.59 ± 0.30
7615	12.22 ± 0.49	7.69 ± 0.27
7616	12.98 ± 1.04	8.41 ± 0.38
7617	12.64 ± 0.50	8.47 ± 0.30
7618	12.89 ± 0.36	8.30 ± 0.21
7620	13.31 ± 0.48	8.33 ± 0.23
7621	13.51 ± 0.48	8.36 ± 0.23
7622	13.52 ± 1.08	8.54 ± 0.38
7623	13.11 ± 0.49	8.93 ± 0.22
7624	13.89 ± 0.52	8.68 ± 0.22
7626	13.31 ± 0.50	8.67 ± 0.21
7627	13.43 ± 0.38	8.67 ± 0.21
7628	13.88 ± 0.50	8.62 ± 0.24
7629	13.11 ± 0.52	8.32 ± 0.29
7631	14.43 ± 0.55	9.08 ± 0.35
7632	13.54 ± 0.61	9.53 ± 0.71
7642	13.95 ± 0.56	9.71 ± 0.34
7643	13.25 ± 0.38	9.66 ± 0.24
7644	13.85 ± 0.35	9.49 ± 0.24
7645	12.74 ± 0.51	9.81 ± 0.34
7648	13.92 ± 0.83	9.63 ± 0.53
7649	13.14 ± 0.39	9.82 ± 0.31
7650	13.35 ± 0.38	10.11 ± 0.25
7652	12.70 ± 0.76	10.27 ± 0.56
7653	13.17 ± 0.53	10.04 ± 0.35
7654	13.17 ± 0.30	9.81 ± 0.20
7655	12.99 ± 0.46	10.07 ± 0.28
7656	13.03 ± 0.43	10.12 ± 0.30
7657	12.72 ± 0.51	9.99 ± 0.35
7658	13.42 ± 0.48	9.62 ± 0.27
7660	11.40 ± 0.46	9.54 ± 0.33
7661	12.49 ± 0.50	9.56 ± 0.48
7663	12.70 ± 0.76	10.56 ± 0.58
7665	12.39 ± 0.50	9.49 ± 0.33
7668	12.35 ± 0.74	9.69 ± 0.53
7673	11.60 ± 0.46	9.72 ± 0.34
7674	11.49 ± 0.46	9.82 ± 0.34
7675	10.77 ± 0.86	9.86 ± 0.44
7676	11.17 ± 0.89	9.31 ± 0.42
7678	11.05 ± 0.29	9.35 ± 0.21
7679	10.60 ± 0.36	9.28 ± 0.27
7680	10.75 ± 0.37	9.76 ± 0.29
7681	10.86 ± 0.31	9.28 ± 0.23
7682	11.44 ± 0.32	9.04 ± 0.22
7683	11.49 ± 0.46	9.45 ± 0.33
7684	10.66 ± 0.43	9.09 ± 0.32
7685	11.28 ± 0.45	8.99 ± 0.31
7686	10.45 ± 0.42	9.25 ± 0.32
7687	10.57 ± 0.85	8.40 ± 0.38
7699	11.19 ± 1.06	7.68 ± 0.46
7700	11.49 ± 1.09	7.68 ± 0.46
7701	11.64 ± 1.11	7.78 ± 0.47
7702	9.97 ± 1.05	8.34 ± 0.29
7703	9.97 ± 0.37	8.73 ± 0.22
7705	10.04 ± 0.40	8.57 ± 0.30
7707	11.08 ± 0.44	8.52 ± 0.30
7708	11.02 ± 0.44	8.57 ± 0.30
7709	11.08 ± 0.44	8.52 ± 0.30
7710	10.99 ± 0.39	8.35 ± 0.23
7711	11.62 ± 0.40	8.64 ± 0.26
7713	11.08 ± 0.67	7.83 ± 0.43
7715	10.51 ± 0.42	8.21 ± 0.29
7716	11.02 ± 0.44	8.54 ± 0.30
7719	11.33 ± 0.45	8.70 ± 0.31
7725	10.99 ± 0.44	9.43 ± 0.33
7728	9.90 ± 0.94	7.93 ± 0.48
7730	10.80 ± 1.03	7.68 ± 0.46
7736	8.09 ± 0.65	8.18 ± 0.37
7741	7.37 ± 0.48	8.01 ± 0.44
7742	7.29 ± 0.58	8.35 ± 0.38
7748	8.06 ± 0.64	8.68 ± 0.39
7749	7.36 ± 0.44	7.54 ± 0.41
7754	7.13 ± 0.43	7.60 ± 0.42
7757	8.81 ± 0.53	7.37 ± 0.41
7758	10.50 ± 0.63	7.60 ± 0.42
7759	9.57 ± 0.57	6.73 ± 0.37
7765	7.83 ± 0.47	6.73 ± 0.37
7766	9.31 ± 0.34	7.10 ± 0.21
7767	9.26 ± 0.31	6.94 ± 0.20
7777	10.24 ± 0.41	7.64 ± 0.27
7778	11.04 ± 0.31	7.90 ± 0.20
7779	10.82 ± 0.43	7.78 ± 0.27
7797	12.20 ± 0.49	8.54 ± 0.30
7809	11.53 ± 0.46	8.76 ± 0.31

TABLE 10

VARIABILITY PARAMETERS

Feature (1)	Mean Flux[a] (2)	F_{var} (3)	R_{max} (4)
F_λ(1350 Å)[b]	43.9	0.32	4.64
F_λ(4870 Å)	11.3	0.14	2.18
Lyα + N v λ1240[b]	76.0	0.17	2.14
Hβ	8.59	0.093	1.57

[a] Units as in Table 9.
[b] From Paper I (GEX values).

tinuum shows the same pattern of variability as seen in the *IUE* data presented in Paper I, and inspection of Figure 3 shows that Hβ, like the ultraviolet emission lines studied in Paper I, also varies in the same pattern but with a short delay. The similarity of the *B*-band measurements, the *IUE* continuum measurements (ultraviolet fluxes and broad-band optical fluxes as measured with the fine-error sensor), and the continuum measurements based on the optical spectra reassures us that our flux calibration is robust.

In Table 10 we present parameters that characterize the amplitude of the optical continuum and Hβ variability. The fractional variation F_{var} is, as defined in Paper I, the ratio of the rms fluctuation to the mean flux, and is corrected for the effect of measurement errors. The parameter R_{max} is the ratio of maximum to minimum flux. Note that both of these parameters are subject to strong systematic effects. While accurate determination of the stellar continuum is very difficult and will be discussed elsewhere, we can make the approximation that at minimum light, about half of the continuum emission through our nominal 5″ × 7″.6 aperture is due to a constant starlight contribution from the host galaxy, and accounting for this will about double the quoted value of F_{var} and increase R_{max} as well. Similarly, the amplitude of variation of Hβ will increase when the constant narrow-line component is taken into account, although this is also true for the ultraviolet lines.

c) *Time-Series Analysis*

Inspection of Figure 3 shows the principal result of this study, namely, that the broad Hβ emission feature varies in the same fashion as the continuum, but with a short delay. These data are replotted in Figure 5, which also shows for comparison purposes the SIPS measurements for the ultraviolet continuum at 1350 Å and the Lyα line (see Paper I for the details of how the ultraviolet measurements were made). Comparison of the light curves for the two emission lines reveals the very important result that they do not vary strictly in phase.

We can quantify the phase shift or "lag" between different light curves by computing their mutual cross-correlations. When the data are unevenly sampled, as they are here, special techniques must be used for these computations. Here we will employ two methods which are commonly used in the context of AGN emission-line variability: (1) the interpolation method of Gaskell and Sparke (1986), with the particular implementation described by Gaskell and Peterson (1987), and (2) the discrete correlation function of Edelson and Krolik (1988). The sampling in this data set is so dense relative to the dominant fluctuation time scales that these two methods give results that are in close agreement.

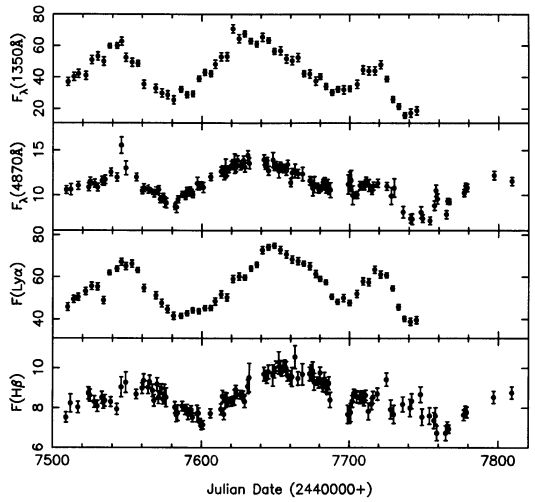

FIG. 5.—Light curves are shown for the ultraviolet (1350 Å) and optical (4870 Å) continua and the Lyα and Hβ emission lines. The continuum fluxes are in units of 10^{-15} ergs s^{-1} cm^{-2} Å^{-1}, and the emission-line fluxes are in units of 10^{-13} ergs s^{-1} cm^{-2}.

i) *Comparison of the Ultraviolet and Optical Continua*

We first investigate the possibility of a phase shift between the ultraviolet and optical continuum by cross-correlating the ultraviolet 1350 Å SIPS light curve from Paper I with the optical continuum light curve presented in Table 9. The result is shown graphically in Figure 6. The peak in the cross-correlation function (CCF) formally occurs at +2 days, in the sense that the optical continuum lags behind the ultraviolet continuum. However, this lag is half the interval between the *IUE* observations, and comparable to the temporal resolution of the optical data, and therefore is probably not significant. We also note that no lag is found between the ultraviolet continuum measurements and the photometric measurements shown in the top panel of Figure 3.

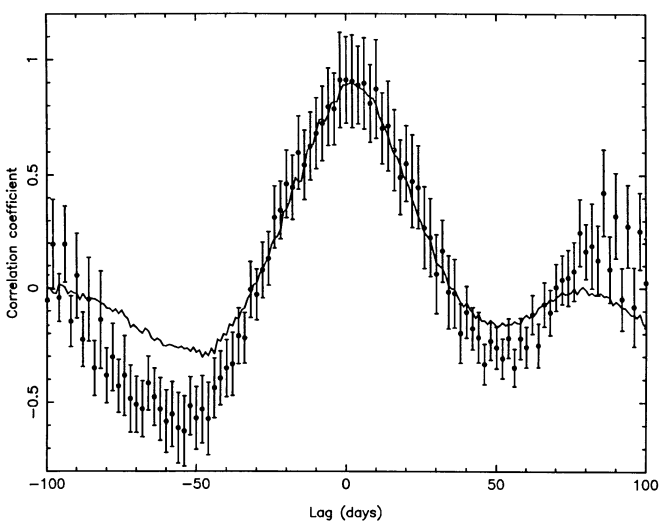

FIG. 6.—Interpolation cross-correlation function, shown as a smooth line, and the discrete correlation function (DCF), shown as individual points with associated uncertainties, for the ultraviolet continuum (1350 Å) and the optical continuum (4870 Å). The optical continuum lags the ultraviolet continuum by ~2 days, which is less than the temporal resolution of this experiment and therefore not significant.

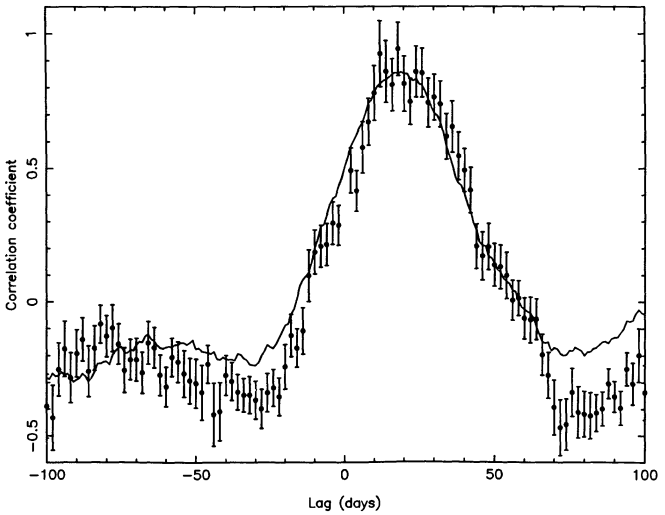

FIG. 7.—Interpolation cross-correlation function and DCF, plotted as in Fig. 6, for the optical continuum and Hβ. The bin width for the DCF is 2 days, since the intercalibration process smooths out variations on shorter time scales. The Hβ emission line lags the optical continuum by about 20 days. The cross-correlation function is broad and flat-topped, and this is attributable to the width of the continuum autocorrelation function, shown in Fig. 8.

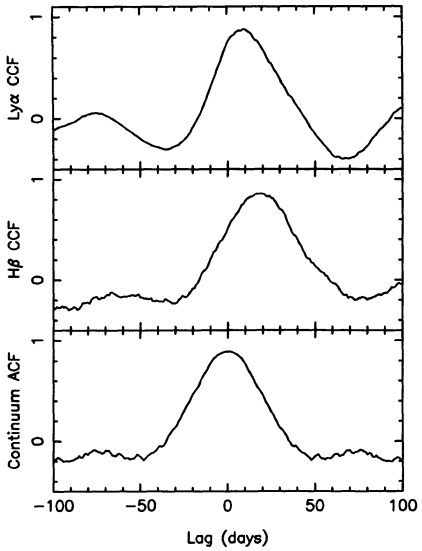

FIG. 8.—*Top panel*: ultraviolet continuum–Lyα cross-correlation function; *middle panel*: optical continuum–Hβ cross-correlation function. The optical continuum autocorrelation function is shown for comparison in the bottom panel.

ii) *Emission-Line Results*

The lag between the optical continuum and Hβ measurements is found to be $\sim$20 days, as seen in Figure 7 and Table 11. This result should be compared with the computed lags for other emission lines as given in Paper I. We note in particular that the lag between the ultraviolet continuum and Lyα is found to be $\sim$10 days. The difference between the response of Lyα and that of Hβ can be substantiated further by a direct cross-correlation of the light curves of these emission lines, from which we find that Hβ lags Lyα by $\sim$8 days. This is consistent with the above results and cross-correlation uncertainties of a few days. The cross-correlation functions for Lyα and Hβ are shown in Figure 8, along with the autocorrelation function (ACF) for the optical continuum. The CCF is the convolution of the transfer function for the BLR and the ACF (see Penston 1990). The similar widths of the CCF and ACF imply that the transfer function itself must be rather narrow compared with the ACF.

iii) *Comments on Uncertainties*

As noted in Paper I, there is no generally accepted method for assigning uncertainties to cross-correlation lags. Moreover, interpreting both the lag and its uncertainty requires knowing or assuming the BLR geometry and orientation. Therefore, we will only note the results of computing the uncertainties from a variety of methods; the important point is that each of these methods indicates that the uncertainty in the lag is small, no worse than a few days. For the sake of simplicity and definiteness, all computations will assume a thin spherical BLR centered on the continuum source, even though this particular geometry is highly unlikely. The sole virtue of this geometry is its simplicity; the transfer function for such a region is specified by a single parameter, the radius.

1. Gaskell and Peterson (1987) give a formula for the uncertainty in the lag, which depends on the width and maximum of the cross-correlation function and the total number of data points. For the cross-correlations summarized in Table 11, errors of $\epsilon \approx 2$ days are indicated by this formula.

2. Maoz and Netzer (1989) use the cross-correlation peak distribution (CCPD) from Monte Carlo simulations to assign an uncertainty to the lag. In our simulations, we start with the optical continuum points given in Table 9 and generate a model light curve by interpolating linearly between observations separated by more than one day and then smoothing this light curve. From this model continuum light curve, we construct a model emission-line light curve by convolving the continuum light curve with the transfer function for the thin spherical shell of radius R. We then resample the model light curves at 127 different points in such a way as to preserve the distribution of intervals between observations. Gaussian-distributed random observational errors are introduced into each of the data points drawn from the model light curves, and the sampled data are then cross-correlated in the same way as real data to determine the location of the peak in the CCF. The CCPD is built up by repeating this process a large number of times for a given value of R. We consider different values of R to find the largest value of R for which a cross-correlation lag no larger than the observed value will be obtained at least a third of the time, and this is adopted as a 1 σ upper limit on the observed size. A similar procedure is followed to find the 1 σ lower limit. The result is 20 ± 3 days for the optical continuum–Hβ cross-correlation.

TABLE 11

CROSS-CORRELATION RESULTS

Parameter (1)	Parameter (2)	Δt_{peak} (days) (3)	r_{max} (4)
F_λ(1350 Å)	F_λ(4870 Å)	2	0.91
F(FES)	F_λ(4870 Å)	2	0.84
F_λ(1350 Å)	$F_\lambda(B)$	0	0.87
F_λ(1350 Å)	F(Lyα)	10	0.88
F_λ(1350 Å)	F(Hβ)	21	0.86
F_λ(4870 Å)	F(Hβ)	19	0.86
F_λ(4870 Å)[a]	F(Hβ)[a]	20	0.86
F(Lyα)	F(Hβ)	8	0.84

[a] Subset from Fig. 2.

3. Each point in the discrete correlation function (DCF) has an associated uncertainty which is derived from the uncertainties in the observed fluxes which contribute to the correlation at a given lag. It is thus possible to perform a meaningful fit to the DCF points near the peak of the function to locate the peak and to estimate the accuracy to which it is known. We have fitted a parabola to the DCF points with correlation amplitudes $r > 0.6$, and we find that the DCF peak occurs at 21.4 ± 3.0 days for the optical continuum–Hβ cross-correlation, at 2.1 ± 0.4 days for the ultraviolet continuum–optical continuum cross-correlation, and at 8.9 ± 1.6 days for the Lyα–Hβ cross-correlation.

It is important to remember at this point that the peak in the CCF for an emission line gives very limited information about the actual geometry of the line-emitting region. More sophisticated techniques, which are beyond the scope of this paper, are required to solve the transfer equation, which contains the information on the BLR geometry. The small uncertainties which we derive for the various CCFs show only that the location of the peak in the CCF is a well-determined quantity. However well determined it is, the lag by itself does not necessarily provide a strong constraint on the distribution of line-emitting material. Moreover, the truly causal connection is with the unobservable ionizing continuum. Based on the cross-correlation between the observed ultraviolet and optical continuum measurements, we believe it likely that the optical continuum tracks the ionizing continuum with a lag of no more than a few days.

V. CONCLUSIONS

An intensive international ground-based campaign to monitor the Seyfert 1 galaxy NGC 5548 has detected the same strong variations observed by the *IUE* satellite during the same period. The combined ultraviolet and optical effort has produced a data base of unprecedented size and quality for studies of AGN variability. On the basis of the initial analysis of these data, we can conclude the following:

1. The optical continuum shows the same qualitative behavior as the ultraviolet continuum. Cross-correlation of the continuum measurements in these two separate wavelength ranges reveals no statistically significant temporal shift between them.

2. The broad Hβ emission line varies in response to the observed continuum variations with a lag of ~ 20 days. It is particularly noteworthy that this lag is significantly longer than the observed lag for Lyα, i.e., ~ 10 days. Direct cross-correlation of the Lyα and Hβ light curves shows a lag of ~ 8 days, which lends credence to this result.

We wish to acknowledge the support and encouragement of numerous members of the AGN community, many of whom were coauthors of Paper I, who made material contributions to the planning of the ground-based program and its *IUE* counterpart. D. Alloin and J. Clavel in particular are thanked for their efforts. Much of the planning and organization of this project took place at the Segovia and Georgia State University conferences in the autumn of 1987, and at IAU Symposium 134 in Santa Cruz in the summer of 1988, and the important role played by the organizers and participants at these conferences is also acknowledged. We are very grateful to the Directors and Telescope Allocation Committees of our various observatories for their support of this demanding project. This project received special support by NASA through a grant administered by the American Astronomical Society, and individual investigators have benefited from support from a number of agencies, including the following: the National Science Foundation: AST-8702691 and AST-8915258 (Ohio State University, AST-8611457 (University of California, Santa Cruz), RII-8800600 and AST-9058510 (University of Arizona), AST-8821839 (University of Florida), AST-8714937 (University of Texas), AST-8957063 and AST-9003829 (University of California, Berkeley), AST-8614510 (University of California), and USE-8750955 (Colgate University under the College Science Instrumentation Program); NASA: NAG5-1366 (Ohio State University), NAS5-29293 (University of Arizona), and NAG5-1194 (Johns Hopkins University); DFG: Bi 191/G-2 and Ko 857/7-1,2 (Universitäts-Sternwarte Göttingen); the National Science and Engineering Research Council of Canada (Mount Royal College); the American Astronomical Society Small Grants Program (Colgate University); and the US–Israel Binational Science Foundation (grant 80/00085 to Wise Observatory). For hospitality extended during part of this investigation, B. M. P. thanks the director and staff of Lick Observatory and M. V. P. acknowledges the Institute of Astronomy. The Isaac Newton telescope is run by the Royal Greenwich Observatory at the Spanish Observatorio del Roque de los Muchachos of the Instituto de Astrofisica de Canarias.

REFERENCES

Clavel, J., *et al.* 1991, *Ap. J.*, in press (Paper I).
Edelson, R. A., and Krolik, J. H. 1988, *Ap. J.*, **333**, 646.
Gaskell, C. M., and Peterson, B. M. 1987, *Ap. J. Suppl.*, **65**, 1.
Gaskell, C. M., and Sparke, L. S. 1986, *Ap. J.*, **305**, 175.
Maoz, D., and Netzer, H. 1989, *M.N.R.A.S.*, **236**, 21.
Maoz, D., *et al.* 1990, *Ap. J.*, **351**, 75.
Netzer, H. 1989, *Comm. Ap.*, **14**, 137.
Netzer, H., *et al.* 1990, *Ap. J.*, **353**, 108.
Oke, J. B., and Gunn, J. E. 1983, *Ap. J.*, **266**, 713.
Penston, M. J., Penston, M. V., and Sandage, A. 1971, *Pub. A.S.P.*, **83**, 783.
Penston, M. V. 1990, in *Variability of Active Galactic Nuclei*, ed. H. R. Miller and P. J. Witta (Cambridge: Cambridge University Press), in press.
Peterson, B. M. 1988, *Pub. A.S.P.*, **100**, 18.
Peterson, B. M., Reichert, G. A., Korista, K. T., and Wagner, R. M. 1990, *Ap. J.*, **352**, 68.
Stone, R. P. S. 1977, *Ap. J.*, **218**, 767.
Wilson, A. S., Wu, X., Heckman, T. M., Baldwin, J. A., and Balick, B. 1989, *Ap. J.*, **339**, 729.

T. J. Balonek and J. A. Christensen: Department of Physics and Astronomy, Colgate University, Hamilton, NY 13346

E. S. Barker, A. L. Cochran, S. R. Sawyer, B. J. Wills, and D. Wills: Department of Astronomy, University of Texas, RLM 15.308, Austin, TX 78712

J. Bechtold and P. S. Smith: Steward Observatory, University of Arizona, Tucson, AZ 85721

R. Bertram and R. M. Wagner: Lowell Observatory, Mars Hill Road, 1400 West, Flagstaff, AZ 86001

N. G. BOCHKAREV: Sternberg State Astronomical Institute, University of Moscow, Universitetskij prosp. 13, Moscow V-234, USSR

M. J. BOLTE: Lick Observatory, University of California at Santa Cruz, Santa Cruz, CA 95064

D. BOND, D. CRAMPTON, J. B. HUTCHINGS, L. SADDLEMYER, and P. F. YOUNGER: Dominion Astrophysical Observatory, 5071 West Saanich Road, Victoria, BC, Canada V8X 4M6

T. A. BOROSON: Kitt Peak National Observatory, National Optical Astronomy Observatories, P.O. Box 26732, Tucson, AZ 85726

M. T. CARINI and H. R. MILLER: Department of Physics and Astronomy, Georgia State University, Atlanta, GA 30303

T. E. CARONE: Space Sciences Laboratory, University of California at Berkeley, Berkeley, CA 94720

S. D. CLEMENTS, R. J. LEACOCK, and A. G. SMITH: Department of Astronomy, University of Florida, Gainesville, FL 32611

R. D. COHEN and E. I. ROSENBLATT: Center for Astrophysics and Space Science, University of California at San Diego, C-011, La Jolla, CA 92093

M. DIETRICH, K. J. FRICKE, and W. KOLLATSCHNY: Universitäts-Sternwarte Göttingen, Geismarlandstrasse 11, D-3400 Göttingen, Federal Republic of Germany

M. ELVIS, J. P. HUCHRA, and B. J. WILKES: Center for Astrophysics, 60 Garden Street, Cambridge, MA 02138

A. FERGUSON and J. H. KROLIK: Department of Physics and Astronomy, Johns Hopkins University, Homewood Campus, Baltimore, MD 21218

A. V. FILIPPENKO, M. W. RICHMOND, and J. C. SHIELDS: Department of Astronomy, University of California at Berkeley, Berkeley, CA 94720

C. M. GASKELL and G. M. MACALPINE: Department of Astronomy, University of Michigan, Dennison Building, Ann Arbor, MI 48109

J. P. HALPERN: Department of Physics, Columbia University, 538 West 120th Street, New York, NY 10027

A. P. KORATKAR: Space Telescope Science Institute, 3700 San Martin Drive, Baltimore, MD 21218

K. T. KORISTA, S. L. MORRIS, and R. J. WEYMANN: Observatories of the Carnegie Institution of Washington, 813 Santa Barbara Street, Pasadena, CA 91101

N. J. LAME, B. M. PETERSON, and R. W. POGGE: Department of Astronomy, The Ohio State University, 174 West 18th Avenue, Columbus, OH 43210

A. LAOR and H. NETZER: School of Physics and Astronomy and the Wise Observatory, Tel-Aviv University, Ramat Aviv, Tel Aviv 69978 Israel

M. A. MALKAN: Department of Astronomy, University of California at Los Angeles, Math-Science Building, Los Angeles, CA 90024

D. MAOZ: Institute for Advanced Study, Princeton, NJ 08540

C. L. M. OLIVEIRA: Department of Astronomy, University of British Columbia, Vancouver, BC, Canada V6T 1W5

J. PENFOLD: Department of Mathematics, Physics, and Engineering, Mount Royal College, Calgary, Alta., Canada T3E 6K6

M. V. PENSTON: Royal Greenwich Observatory, Madingley Road, Cambridge CB3 0EZ, United Kingdom

E. PÉREZ: Instituto de Astrofísica de Canarias, E-38200 La Laguna, Tenerife, Spain

W. ROMANISHIN: Department of Physics and Astronomy, University of Oklahoma, Norman, OK 73019

A. SADUN: Department of Physics and Astronomy, Bradley Observatory, Agnes Scott College, Decatur, GA 30030

A. I. SHAPOVALOVA: Special Astrophysical Observatory, USSR Academy of Sciences, Nizhni Arkhys Stavropolsky Kraj, 357140 USSR

H. A. SMITH: Department of Astronomy, Michigan State University, East Lansing, MI 48824

W.-H. SUN: Institute of Physics and Astronomy, National Central University, 32054 Chung-li, Taiwan

U. THIELE: Max-Planck-Institut für Astronomie, Koenigstuhl, D-6900 Heidelberg, Germany

T. J. TURNER: Laboratory for High Energy Astrophysics, Goddard Space Flight Center, Greenbelt, MD 20771

S. VEILLEUX: Institute for Astronomy, University of Hawaii, 2680 Woodland Drive, Honolulu, HI 96822